NASA TECHNICAL NOTE

NASA TN D-2033

NASA TN D-2033

TRANSONIC INVESTIGATION OF A PYRAMIDAL REENTRY CONFIGURATION WITH CAMBERED VARIABLE-SWEEP WINGS AND VARIOUS LONGITUDINAL CONTROLS

by Bernard Spencer, Jr.

Langley Research Center,
Langley Station, Hampton, Va.

NATIONAL AERONAUTICS AND SPACE ADMINISTRATION • WASHINGTON, D. C. • DECEMBER 1963

TECHNICAL NOTE D-2033

TRANSONIC INVESTIGATION OF A PYRAMIDAL REENTRY CONFIGURATION WITH CAMBERED VARIABLE-SWEEP WINGS AND VARIOUS LONGITUDINAL CONTROLS

By Bernard Spencer, Jr.

Langley Research Center
Langley Station, Hampton, Va.

NATIONAL AERONAUTICS AND SPACE ADMINISTRATION

TRANSONIC INVESTIGATION OF A PYRAMIDAL REENTRY CONFIGURATION WITH CAMBERED VARIABLE-SWEEP WINGS AND VARIOUS LONGITUDINAL CONTROLS

By Bernard Spencer, Jr.

SUMMARY

An investigation has been conducted in the Langley high-speed 7- by 10-foot tunnel at Mach numbers from 0.40 to 1.13 on a blunted right-triangular pyramidal lifting reentry configuration employing highly cambered variable-sweep wings as a method of increasing lift and lift-drag ratio at subsonic speeds. The angle-of-attack range of the investigation was from approximately -1° to 25° at zero sideslip angle. Longitudinal control was provided by a body-base trailing-edge flap, a canard control located at the body apex, and an afterbody flap simulating model base boattailing.

Unsweeping the wing panel from 80° to 0° leading-edge sweep at a Mach number of 0.40 resulted in an increase in lift-curve slope from 0.0170 to 0.0540, an increase in maximum untrimmed lift-drag ratio from 2.7 to 5.2, and only slight changes in the level of static margin. Losses in lift for the 0° leading-edge sweep wing above an angle of attack of 8° tended to reduce the desirability of this configuration in the range of possible landing attitudes (between 12° and 16°). The configuration having wing panels swept back 40° had the highest values of lift coefficient and lift-drag ratio in this attitude range. For the configuration having wing panels swept back 80°, a comparison of the longitudinal control characteristics at a Mach number of 0.40 for body trailing-edge flaps, canard leading- and trailing-edge flaps, and afterbody flap controls indicates that the afterbody flaps provided the highest values of trimmed lift-drag ratio for the range of trimmed lift coefficients obtained. A comparison of the trimmed lift, lift-drag ratio, and corresponding angle of attack for the basic configuration (with wing panels swept back 80°) and the configuration having 40° of sweep indicates gains in trimmed values of lift-drag ratio realized from extending the wing panel to 40° sweep, with correspondingly large reductions in trimmed angle of attack for given values of lift coefficient.

INTRODUCTION

The National Aeronautics and Space Administration is currently conducting general research programs on various low-aspect-ratio lifting reentry configurations to determine the aerodynamic characteristics of such vehicles at landing

speeds up to hypersonic entry velocities. In an effort to attain desirable landing characteristics for such vehicle concepts, various types of variable geometry have been applied to basic configurations which were designed from reentry considerations. The use of variable geometry has indicated that significant gains in lift and lift-drag ratio are obtainable at subsonic speeds. (See refs. 1 to 3.) Lift and lift-drag ratio are, of course, both significant factors during the landing maneuver. The basic configuration of reference 2, which was a blunted right-triangular pyramidal lifting configuration, has exhibited satisfactory longitudinal and lateral stability characteristics from hypersonic to low subsonic speeds. (See refs. 4 to 7.) The use of variable-sweep wing panels on this configuration also produced large gains in maximum lift-drag ratio and lift variation with angle of attack. However, stalling of the wing panel in a 0° leading-edge sweep condition at moderate angles of attack restricted the usable lift range for this configuration. These losses in lift occurred well below desirable landing attitudes ($\alpha \approx 16^\circ$).

The problem of providing longitudinal control for most reentry lifting-body shapes arises from the fact that the basic shape is usually of low span and fairly compact in length, resulting in relatively short moment arms for the controls. Owing to the large deflections required for trim at high lift coefficients, considerable loss in lift and lift-drag ratio has been noted for controls located behind the moment reference point because of the negative increment in lift required for trim and the resultant increased trim drag. If, however, a more efficient control location could be employed, considerable reduction in the trim drag penalties should be realized.

The purpose of the present investigation was to provide information on the longitudinal aerodynamic characteristics at subsonic and transonic speeds on a blunted right-triangular pyramidal lifting reentry configuration having a more highly cambered variable-sweep wing panel than the flat-bottom modified NACA 0024 airfoil section used in reference 2. Also presented is a comparison of the longitudinal control characteristics of a configuration in combination with a body trailing-edge flap, a canard-type control, and afterbody flaps located at the body base. The tests were conducted in the Langley high-speed 7- by 10-foot tunnel at Mach numbers from 0.40 to 1.13 corresponding to a range of average test Reynolds numbers, based on the body ridge line length, from 4.3×10^6 to 7.5×10^6. The angle-of-attack range was varied from -1° to 25° at zero sideslip angle.

SYMBOLS

All data presented herein are referred to the wind-axis system, and all forces and moments are nondimensionalized with respect to the ridge line length and the projected planform area of the configuration having wing panel fully swept back ($\Lambda_{le} = 80^\circ$). Unless otherwise noted, the moment reference point was located 9.50 inches ahead of the model base and 1.21 inches below the model upper surface for all tests.

A	aspect ratio, b^2/S
b	configuration span when wing panels are folded and $\Lambda_{le} = 80^\circ$, ft
C_D	drag coefficient, $\frac{\text{Drag}}{qS}$
C_L	lift coefficient, $\frac{\text{Lift}}{qS}$
C_{L_α}	lift-curve slope, per deg ($\alpha \approx 0^\circ$)
C_m	pitching-moment coefficient, $\frac{\text{Pitching moment}}{qSc}$
$\frac{\partial C_m}{\partial C_L}$	longitudinal stability parameter
c	model ridge line length, ft
L/D	lift-drag ratio
$(L/D)_{max}$	maximum lift-drag ratio
M	Mach number
q	dynamic pressure, lb/sq ft
S	reference area, sq ft
α	angle of attack, deg
δ_A	afterbody flap deflection, positive with trailing edge moving toward model center line, deg
δ_f	body trailing-edge flap deflection, positive with trailing edge down, deg
$\delta_{n,c}$	canard leading-edge flap deflection, positive with flap leading edge up, deg
$\delta_{f,c}$	canard trailing-edge flap deflection, positive with flap trailing edge down, deg
Λ_{le}	wing-panel leading-edge sweep, deg

Model Components

WB	wing-body configuration (all controls off)
C	canard control
F	body trailing-edge flap
A	afterbody flaps

MODEL

The basic configuration of the present investigation was a blunted right-triangular pyramid with wing panels folded 80°, and all longitudinal controls off. Geometric characteristics of the body are presented in figure 1. Also included in figure 1 is a listing of the reference area and lengths. A photograph of the model with the 20° sweptback wing panels, the canard, the trailing-edge flap control, and the afterbody flap control mounted on the basic body is presented as figure 2.

The wing panels of the present tests were highly cambered in section, with the upper and lower surfaces represented by arcs of circles as indicated in figure 1. The wing leading-edge radius was approximately the same as the body leading-edge radius, as measured normal to the body leading edge. The wing panels were untapered with the pivot point located at 56.3 percent of the body length. Leading-edge wing-panel sweeps of 0°, 20°, 40°, 60°, and 80° were employed.

Details of the longitudinal controls are also included in figure 1. The trailing-edge flap control was an untapered flat plate, attached to the upper edge of the model base, with a maximum deflection of -40°. The ratio of the flap area to the reference area was approximately 0.0379. The canard, which had its apex located at the body apex, was a 0.10-inch-thick flat plate with a rounded leading edge and a blunt trailing edge. Deflectable leading- and trailing-edge flaps were employed on the canard with the hinge lines for the leading- and trailing-edge flaps located along the 20- and unswept 80-percent-chord lines, respectively.

The afterbody flaps, which were designed to be deflected from the body base, had a ratio of the flap area (both flaps) to the reference area of 0.0938. Flap deflections of 90°, 100°, 110°, and 120° were used, with the 90° flap deflection being considered as the case in which the flaps were an extension of the dihedral surfaces of the body. (See fig. 1.)

TESTS AND CORRECTIONS

The present investigation was conducted in the Langley high-speed 7- by 10-foot tunnel at Mach numbers from 0.40 to 1.13, corresponding to a range of

average test Reynolds numbers, based on the model ridge line, from 4.5×10^6 to 7.5×10^6. The model was sting supported, and the forces and moments were measured by use of a six-component internally mounted strain-gage balance.

The model was tested through an angle-of-attack range from approximately -1° to 25° at zero sideslip angle.

Corrections to the angle of attack due to sting and balance deflection under load have been applied to the data. No attempt was made to fix transition on the model. No corrections for the effects of base pressure have been applied to the data, since the configuration is considered as an unpowered gliding vehicle.

RESULTS AND DISCUSSION

Figure 3 presents longitudinal aerodynamic data for the basic configuration and figures 4 to 9 present the data for the basic configuration with various combinations of model components tested. A summary of the longitudinal aerodynamic characteristics and longitudinal control effectiveness characteristics is presented in figures 10 to 14. Most of the discussion will be confined to the summary figures, with pertinent observations noted from the basic data.

The effects of unsweeping the wing panels from a fully retracted position $(\Lambda_{le} = 80^\circ)$ to various leading-edge positions at Mach numbers from 0.40 to 1.13 are presented in figure 3 for the configuration with all controls off. Unsweeping the wing panel from 80° to 0° at a Mach number of 0.40 resulted in an increase in lift-curve slope from 0.0170 to 0.0540, an increase in maximum untrimmed lift-drag ratio from 2.7 to 5.2, and only slight changes in static margin. (See figs. 3 and 11.) An increase in lift coefficient from 0.07 to 0.45 at $\alpha = 0^\circ$ is realized by unsweeping the wing panels from $\Lambda_{le} = 80^\circ$ to $\Lambda_{le} = 0^\circ$ at $M = 0.40$. Above an angle of attack of 8°, losses in lift-curve slope for the wing panels in the 0° leading-edge sweep position occur owing to flow separation at the lowest test Mach number. (See fig. 3(a).) Above $\alpha \approx 11^\circ$, losses in lift-curve slope for the $\Lambda_{le} = 20^\circ$ wing are also indicated, with the result that above $C_L = 0.92$ the $\Lambda_{le} = 40^\circ$ configuration gave the highest values of C_L and L/D. A comparison of the lift characteristics of the present cambered airfoil section with those of the airfoil section of reference 2 indicates an increase in C_L of approximately 0.10 $(0^\circ < \alpha < 8^\circ)$ for the present airfoil, with considerable improvement in lift-drag ratio in the lift-coefficient range above $C_L = 0.70$. Further improvement in C_L may be realized from use of wing leading-edge devices to delay flow separation over the wing with resultant improvements in the lift-drag ratio at the higher lift coefficients $(C_L = 1.0)$ which are desirable from landing considerations. For the present investigation, however, the configuration having a wing leading-edge sweep of 40° provides the highest values of C_L in the region of possible landing attitudes ($\alpha = 12^\circ$ to 18°).

Summary of the effects of Mach number on the configuration at various wing-panel sweeps (fig. 10) indicates losses in $(L/D)_{max}$ for the low and moderate sweep configurations as Mach number is increased. These losses are accompanied by losses in lift-curve slope and low-lift stability due, of course, to the increasing Mach number exceeding the critical Mach number for this thick airfoil section. It is interesting to note, however, from comparison of the low-lift stability level for the 20° sweep configuration at $M = 0.40$ and the 80° sweep configuration at $M = 1.13$, that the stability levels are approximately the same. These results are generally in agreement with those of reference 2 for a similar configuration.

The effects of the addition of the undeflected canard and trailing-edge flap to the basic body having various wing-panel sweeps on the longitudinal aerodynamic parameters C_{L_α}, $(L/D)_{max}$, and $\partial C_m/\partial C_L$ at $M = 0.40$ are indicated in figure 11. Throughout the test range of wing-panel sweep, only slight effects on C_{L_α} and $(L/D)_{max}$ result from the addition of either the trailing-edge flap or the canard at zero deflection. The addition of the trailing-edge flap to the basic configuration causes decreases in $\partial C_m/\partial C_L$ at the high wing-panel sweeps and, generally, slight increases in $\partial C_m/\partial C_L$ at the low wing-panel sweeps. As would be expected, the addition of the canard surface resulted in large destabilizing moments at all wing-panel sweeps.

In order to provide a reasonable comparison of control effectiveness for the trailing-edge flap, canard, and afterbody flap, the low-lift stability for the three configurations has been adjusted to give approximately equal static margin (-0.03c) and the resultant L/D and C_m variations with increasing C_L are presented as figure 12 for the $\Lambda_{le} = 80^{\circ}$ configuration at a Mach number of 0.40. Deflection of the afterbody flap controls provides trimmed lift coefficients to approximately 0.68, with only a slight reduction in lift-drag ratio caused by flap deflection. The positive moment provided by deflection of this flap occurs as a result of the negative lift increment accompanying flap deflection (fig. 4). There is also a reduction in base drag due to the boattailing effect from inward deflection of these flaps. The slight loss in lift and positive moments produced by deflection of these flaps, combined with the reduction in base drag, are the reasons for only slight losses in trimmed lift-drag ratio due to flap deflection. The large reductions in L/D, realized from deflection of the body trailing-edge flap as illustrated in figure 12, imply that trimmed L/D for any value of C_L is less than that obtained with the afterbody flaps. Deflection of the canard leading- and trailing-edge flaps provides only small values of positive moment and, because of the large forward movement of moment reference required to provide a stable configuration at low lifts, appears to be of little value for the present configuration. It is interesting to note, however, that the maximum lift-drag ratio of the deflected-canard configuration is higher than that of the undeflected-canard configuration.

The effects of increasing Mach number on the basic configuration $(\Lambda_{le} = 80^{\circ})$, on the configuration having trailing-edge and afterbody flap controls, and on the configuration having canard and afterbody flap controls are presented in

figure 13. At a given Mach number, there is little or no effect on C_{L_α} or $(L/D)_{max}$ caused by the addition of the various controls to the basic body $(\Lambda_{le} = 80^\circ)$. The large destabilizing moment produced by addition of the canard is approximately 0.12c throughout the Mach number range of this investigation.

In an effort to illustrate the improvements in trimmed lift and lift-drag ratio which are realized by unsweeping the variable-sweep wing panels, a comparison of the longitudinal trim characteristics of the $\Lambda_{le} = 40^\circ$ and $\Lambda_{le} = 80^\circ$ configurations is presented in figure 14, for a Mach number of 0.40, with the moment reference adjusted to give approximately -0.12c for each configuration. Longitudinal control was provided, in each case, by deflection of the body trailing-edge controls, with the afterbody flaps on $(\delta_A = 120^\circ)$. (See figs. 5(a) and 5(b) for basic untransferred data.)

Improvements in trimmed lift-drag ratio for a given value of C_L are realized by unsweeping the wing panels from 80° to 40° (fig. 14). More significant, however, are the large reductions in the trimmed angle of attack for given values of lift coefficient - a factor which becomes increasingly important when landing attitudes are restricted because of pilot vision or ground-clearance considerations.

SUMMARY OF RESULTS

An investigation has been conducted in the Langley high-speed 7- by 10-foot tunnel at Mach numbers from 0.40 to 1.13 on a blunted right-triangular pyramidal lifting reentry configuration employing highly cambered variable-sweep wings as a method of obtaining high lift and lift-drag ratio at subsonic speeds. Longitudinal control was provided by a base trailing-edge flap, a canard which had leading- and trailing-edge flaps and was located at the body apex, and an afterbody flap simulating base boattailing. Results of the investigation may be summarized as follows:

1. Unsweeping the wing panel from 80° to 0° leading-edge sweep at a Mach number of 0.40 resulted in an increase in lift-curve slope from 0.0170 to 0.0540, an increase in maximum untrimmed lift-drag ratio from 2.7 to 5.2, and only slight changes in the level of static margin. Losses in lift for the 0° leading-edge sweep wing above an angle of attack of 8° tended to reduce the desirability of this configuration in the range of possible landing attitudes (between 12° and 16°). The configuration having wing panels swept back 40° had the highest values of lift coefficient and lift-drag ratio in this attitude range.

2. For the configuration having wing panels swept back 80°, a comparison of the longitudinal control characteristics at a Mach number of 0.40 for body trailing-edge flaps, canard leading- and trailing-edge flaps, and afterbody flap controls indicates that the afterbody flap control provided the highest values of trimmed lift-drag ratio for the range of trimmed lift coefficients obtained.

3. A comparison of the trimmed lift, lift-drag ratio, and corresponding angle of attack for the basic configuration (with wing panels swept back 80°) and the configuration having 40° of sweep indicates gains in trimmed values of lift-drag ratio realized from extending the wing panel to 40° sweep, with correspondingly large reductions in trimmed angle of attack for given values of lift coefficient.

Langley Research Center,
National Aeronautics and Space Administration,
Langley Station, Hampton, Va., August 26, 1963.

REFERENCES

1. McLellan, Charles H., and Ladson, Charles L.: A Summary of the Aerodynamic Performance of Hypersonic Gliders. NASA TM X-237, 1960.

2. Spencer, Bernard, Jr.: Longitudinal Aerodynamic Characteristics at Mach Numbers From 0.40 to 1.10 of a Blunted Right-Triangular Pyramidal Lifting Reentry Configuration Employing Variable-Sweep Wing Panels. NASA TN D-1518, 1963.

3. Smith, Willard G.: A Wind-Tunnel Investigation at Subsonic and Low Supersonic Speeds of a Reentry Vehicle With Retractable Wings. NASA TM X-398, 1961.

4. Mayo, Edward E.: Static Longitudinal Stability Characteristics of a Blunted Glider Reentry Configuration Having 79.5° Sweepback and 45° Dihedral at a Mach Number of 6.2 and Angles of Attack up to 20°. NASA TM X-222, 1959.

5. Whitcomb, Charles F., and Foss, Willard E., Jr.: Static Stability and Control Characteristics of Two Large-Dihedral Right Triangular Pyramid Lifting Reentry Configurations at a Mach Number of 3.05. NASA TM X-295, 1960.

6. Ware, George M.: Low-Subsonic-Speed Static Stability of Right-Triangular-Pyramid and Half-Cone Lifting Reentry Configurations. NASA TN D-646, 1961.

7. Olstad, Walter B., Mugler, John P., Jr., and Cahn, Maurice S.: Static Longitudinal and Lateral Stability Characteristics of a Right Triangular Pyramidal Lifting Reentry Configuration at Transonic Speeds. NASA TN D-655, 1961.

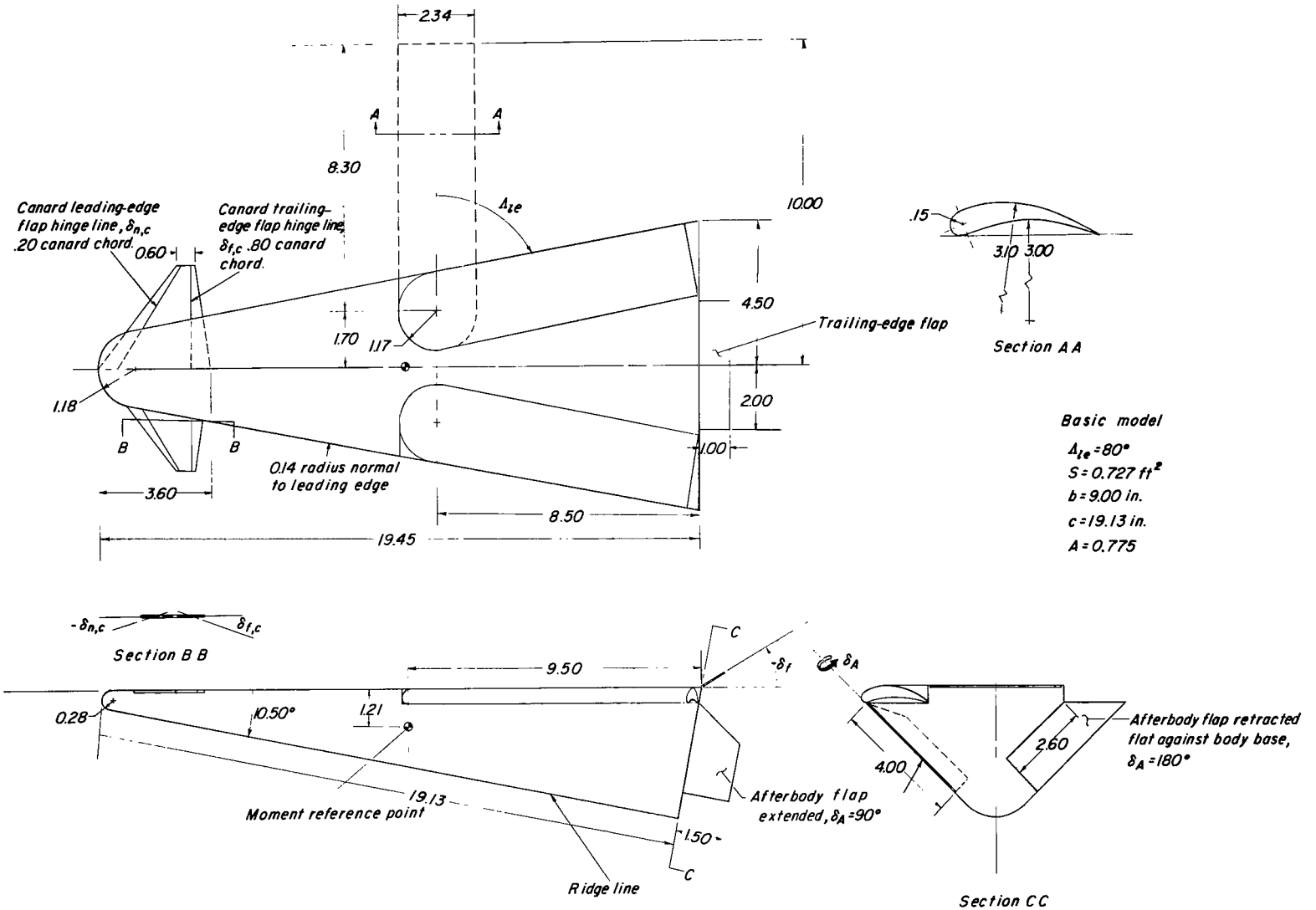

Figure 1.- Geometric characteristics of models. All linear dimensions are in inches unless otherwise noted.

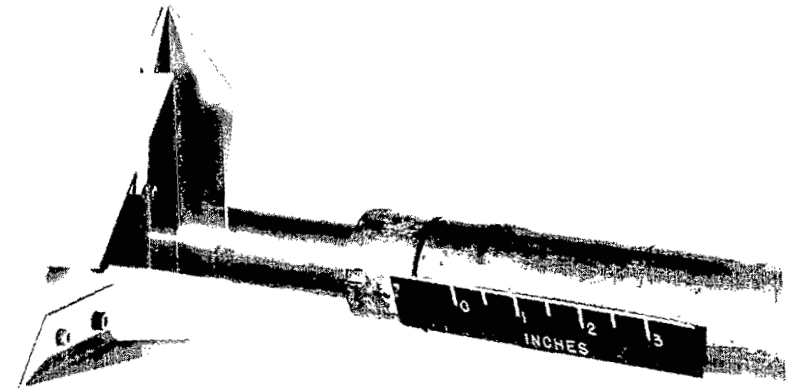

L-63-485

Figure 2.- Photograph of basic body with canard, trailing-edge flaps, afterbody flaps, and variable-sweep wing panels. $\Lambda_{le} = 20^{\circ}$.

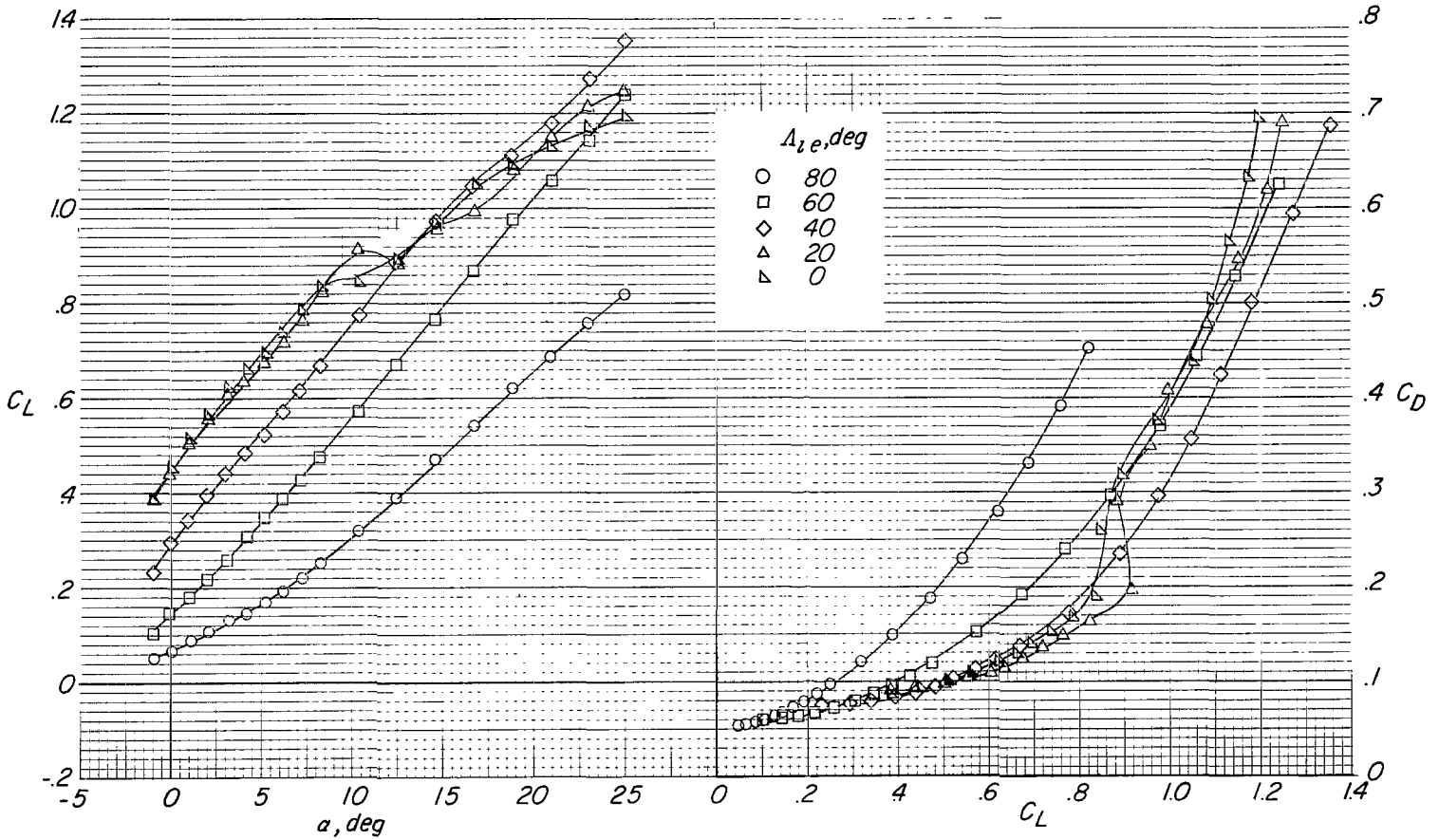

(a) M = 0.40.

Figure 3.- Effects of wing-panel sweep on longitudinal aerodynamic characteristics of basic configuration at various Mach numbers. All longitudinal controls off.

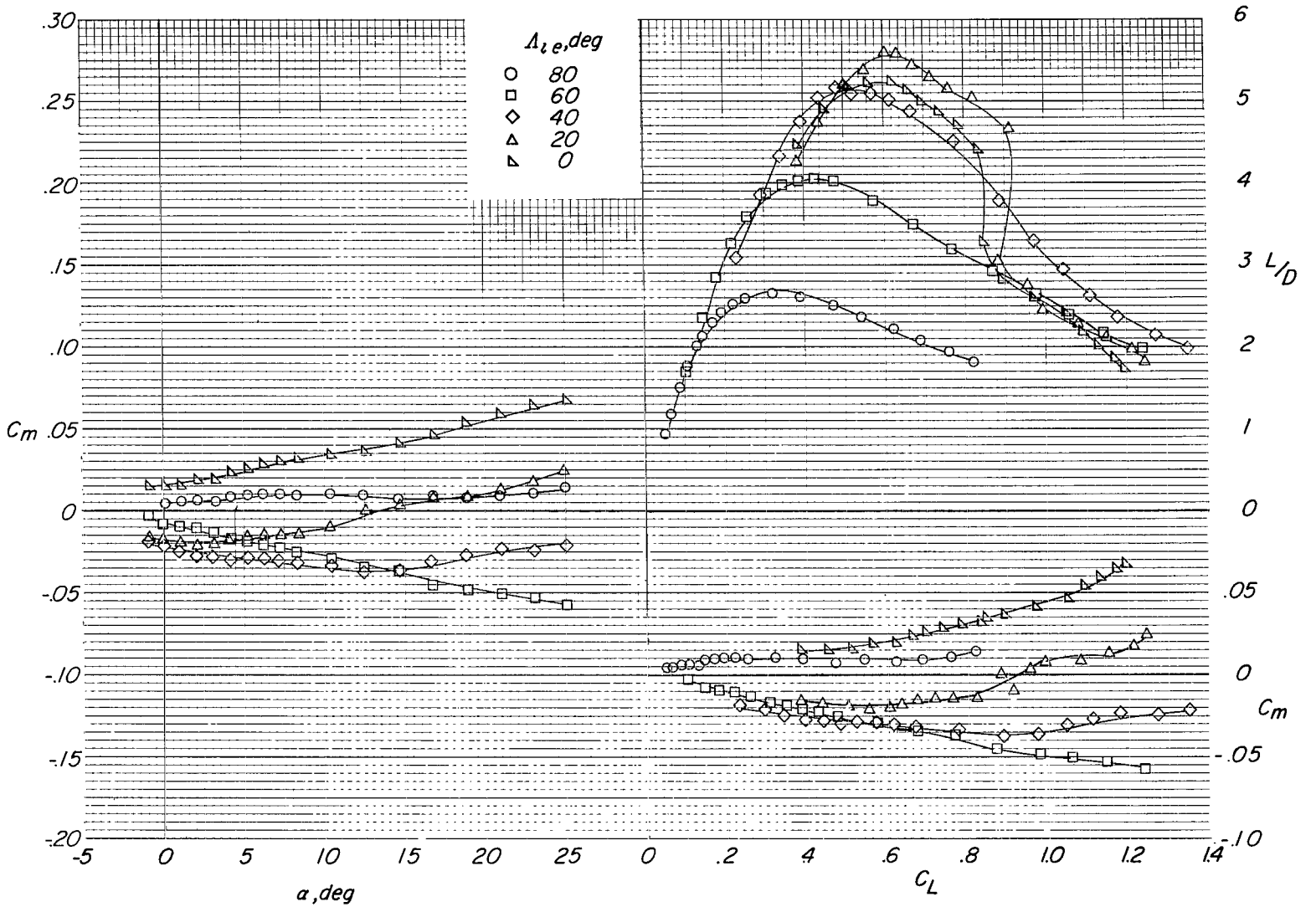

(a) M = 0.40. Concluded.

Figure 3.- Continued.

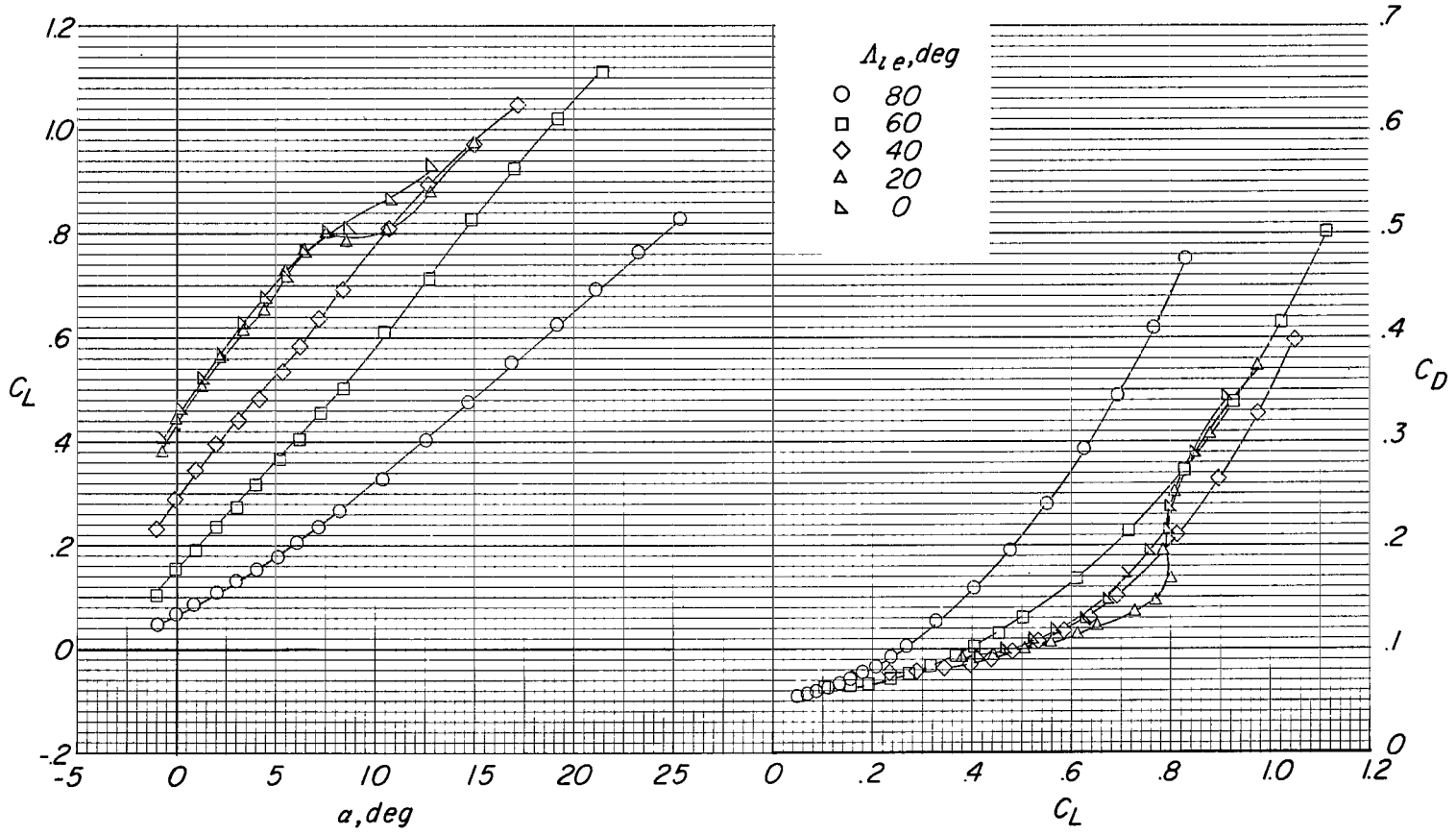

(b) M = 0.60.

Figure 3.- Continued.

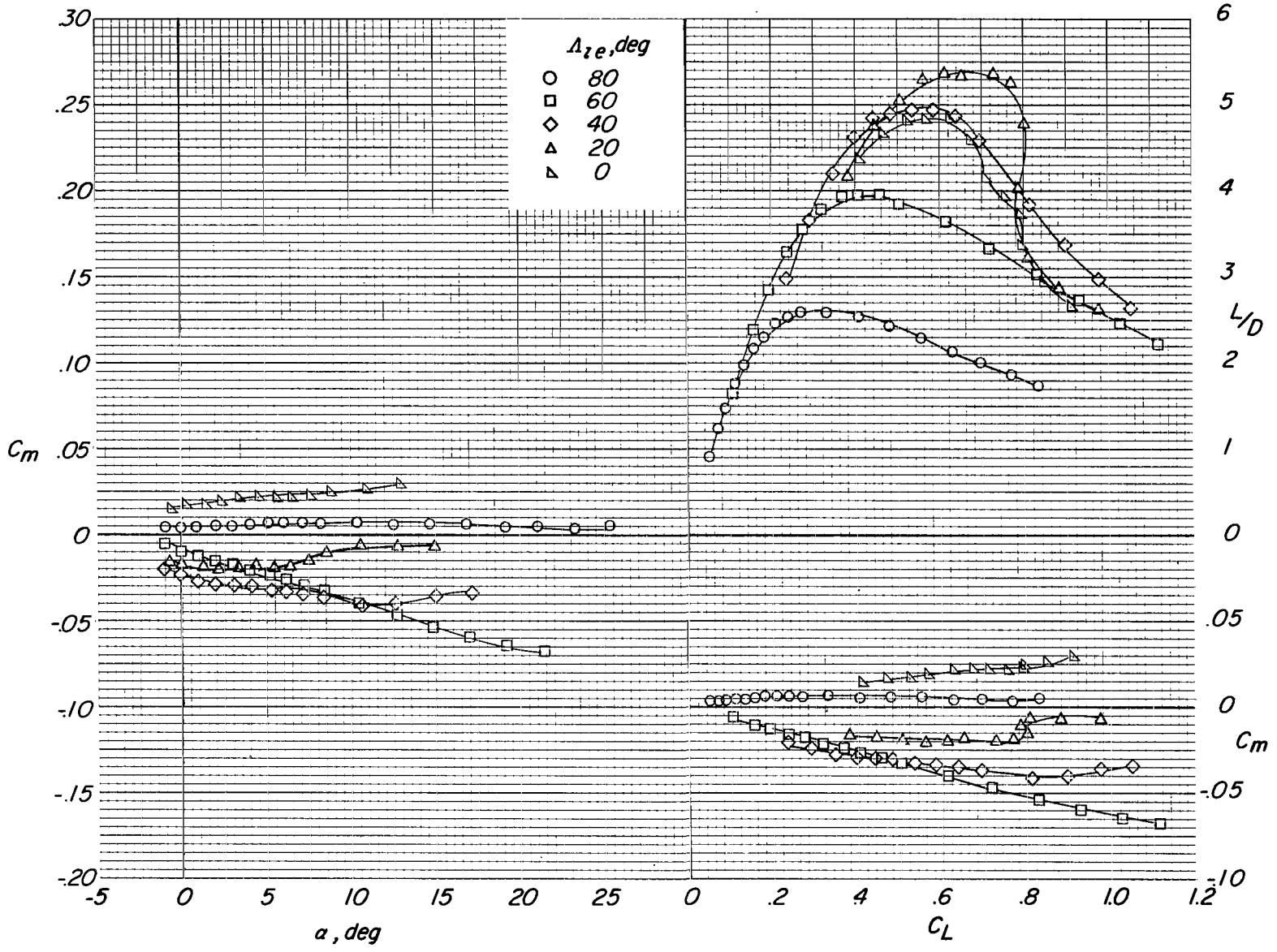

(b) M = 0.60. Concluded.

Figure 3.- Continued.

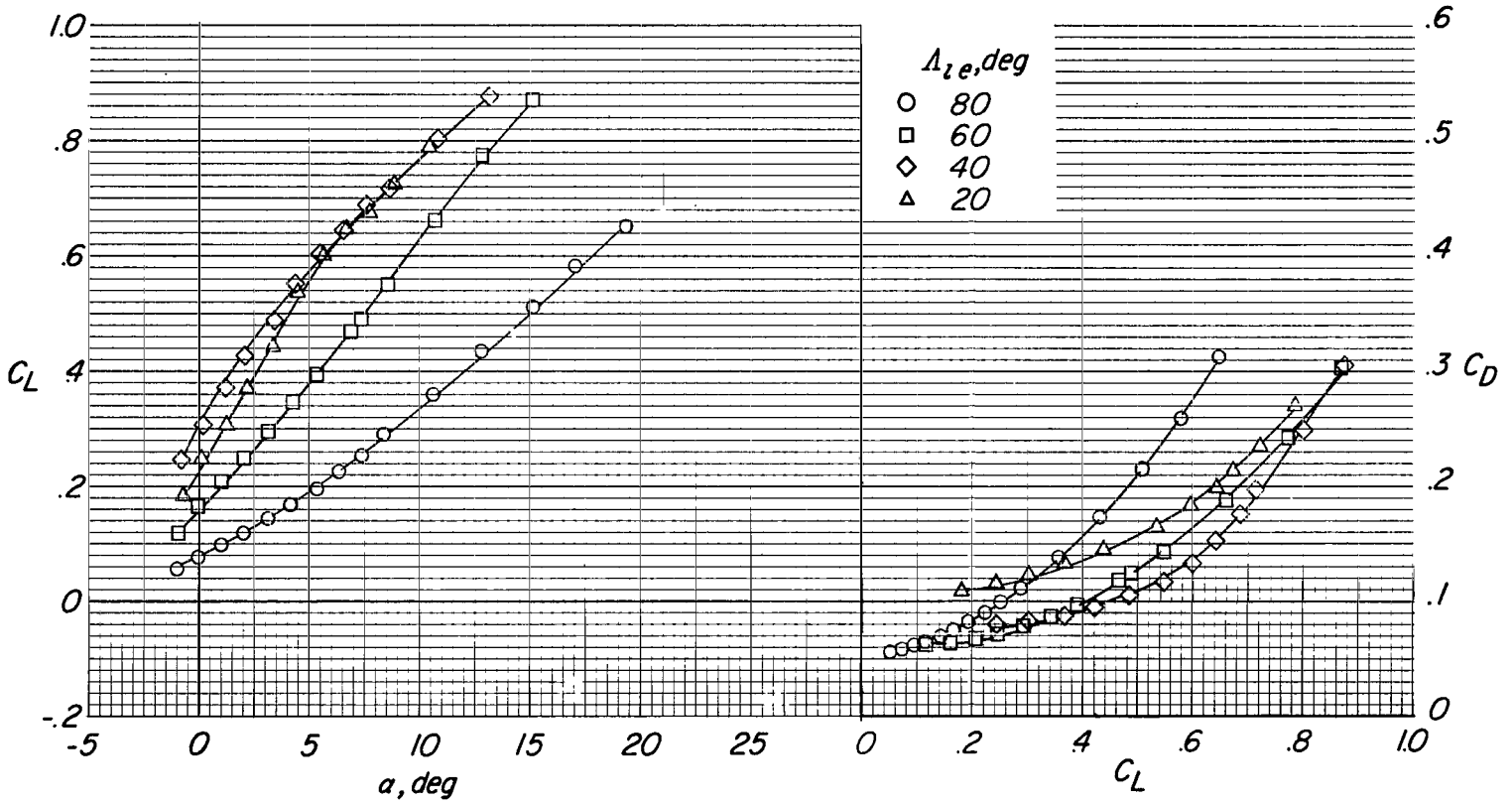

(c) M = 0.80.

Figure 3.- Continued.

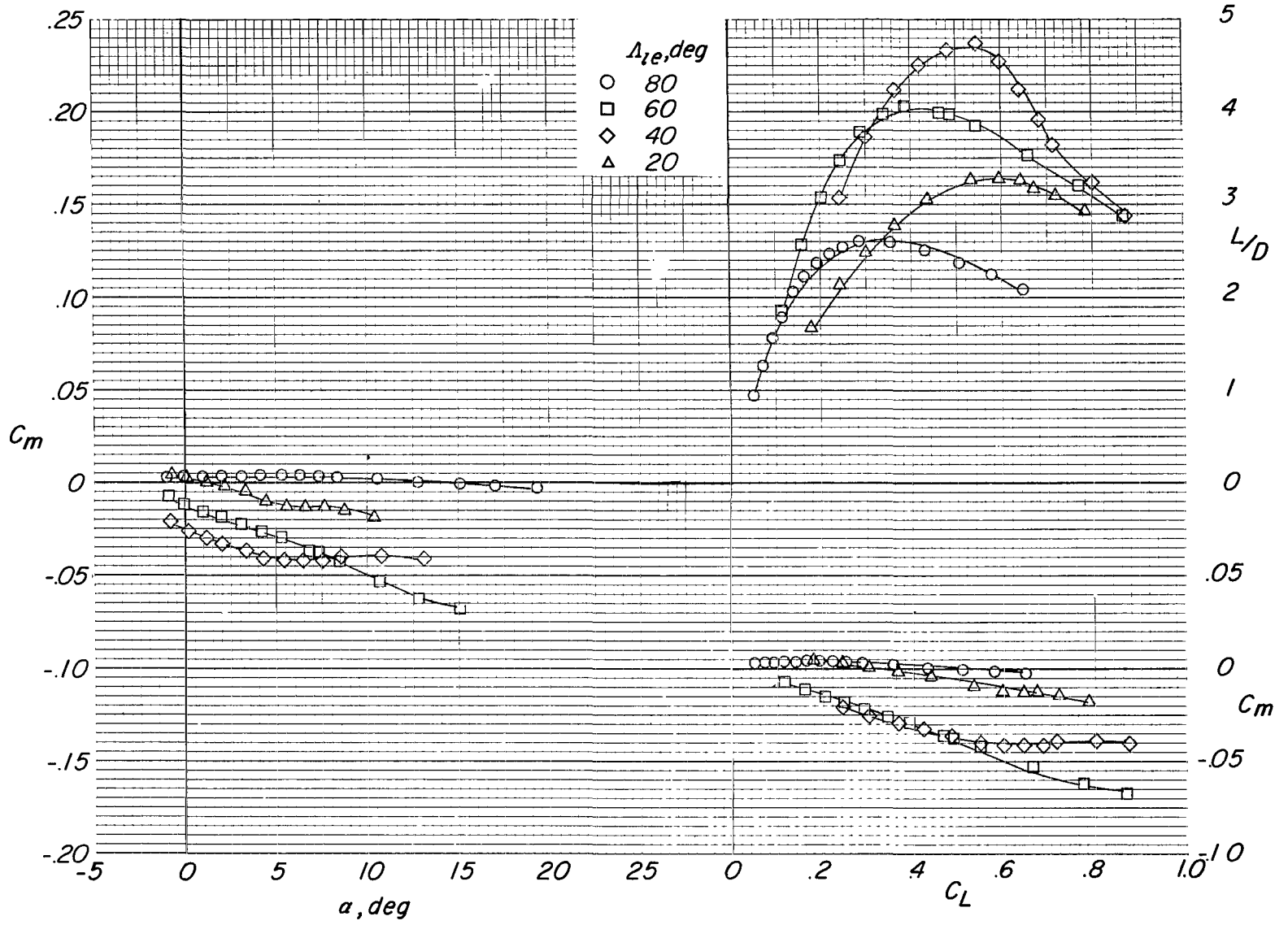

(c) M = 0.80. Concluded.

Figure 3.- Continued.

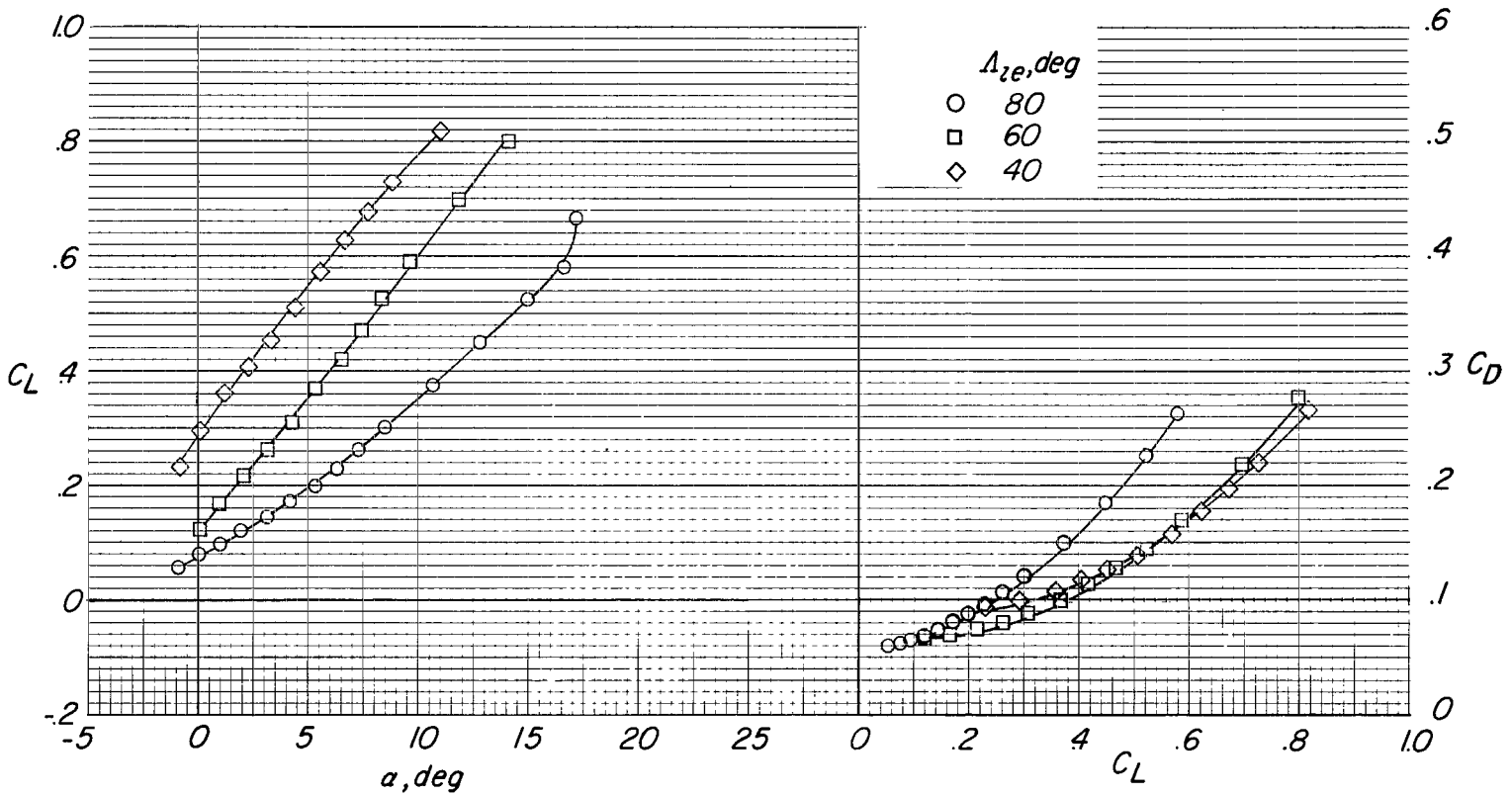

(d) M = 0.90.

Figure 3.- Continued.

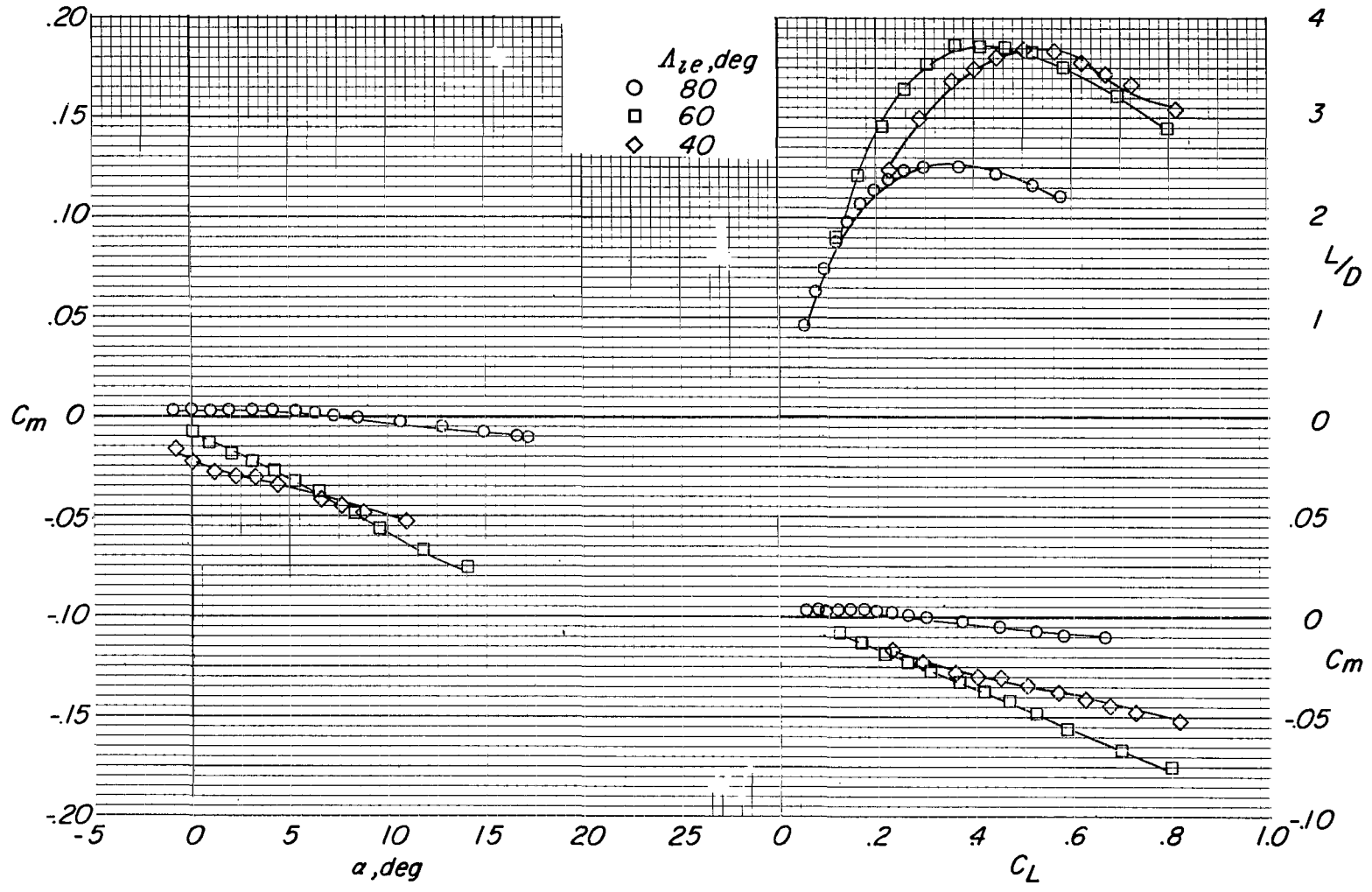

(d) M = 0.90. Concluded.

Figure 3.- Continued.

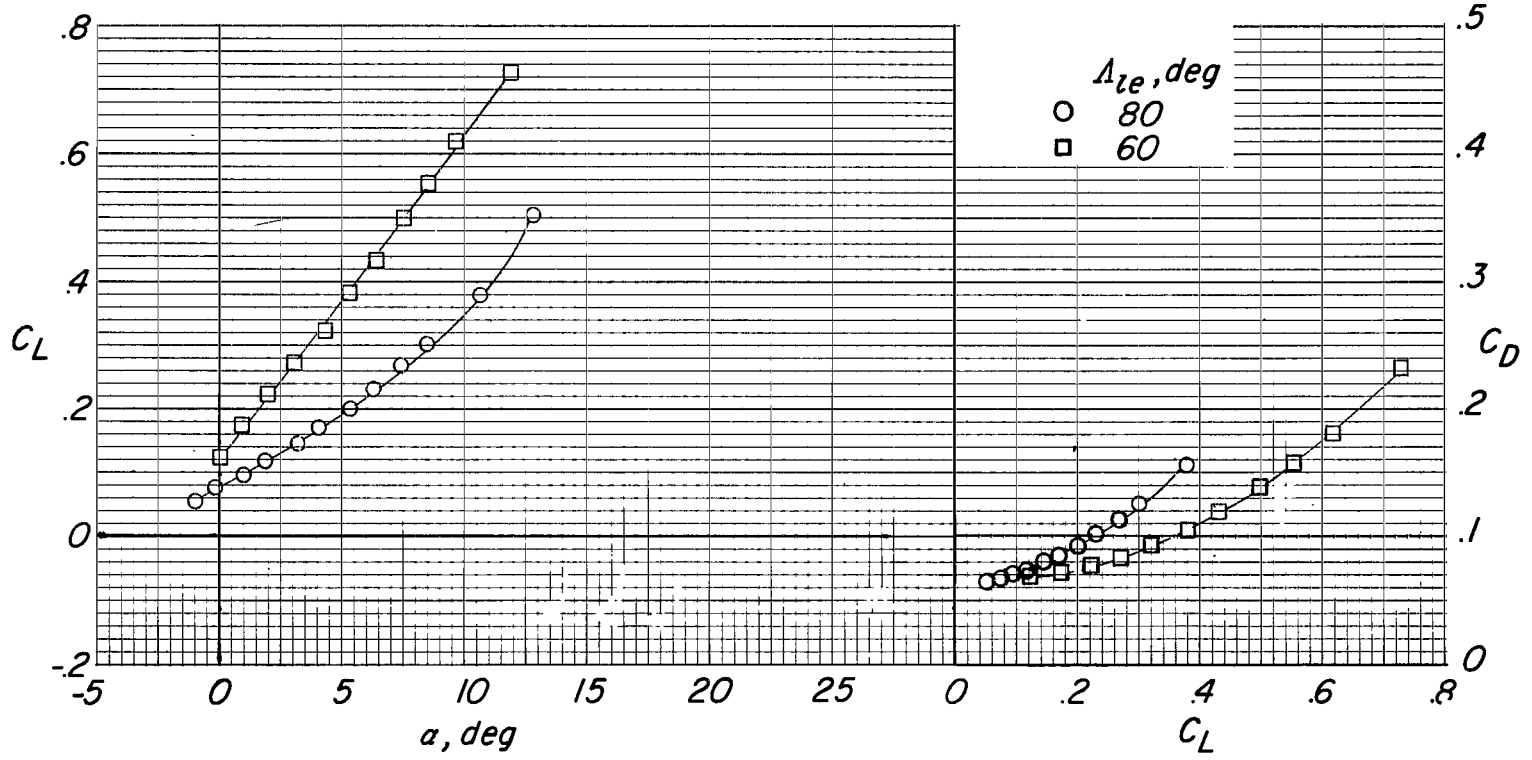

(e) M = 0.95.

Figure 3.- Continued.

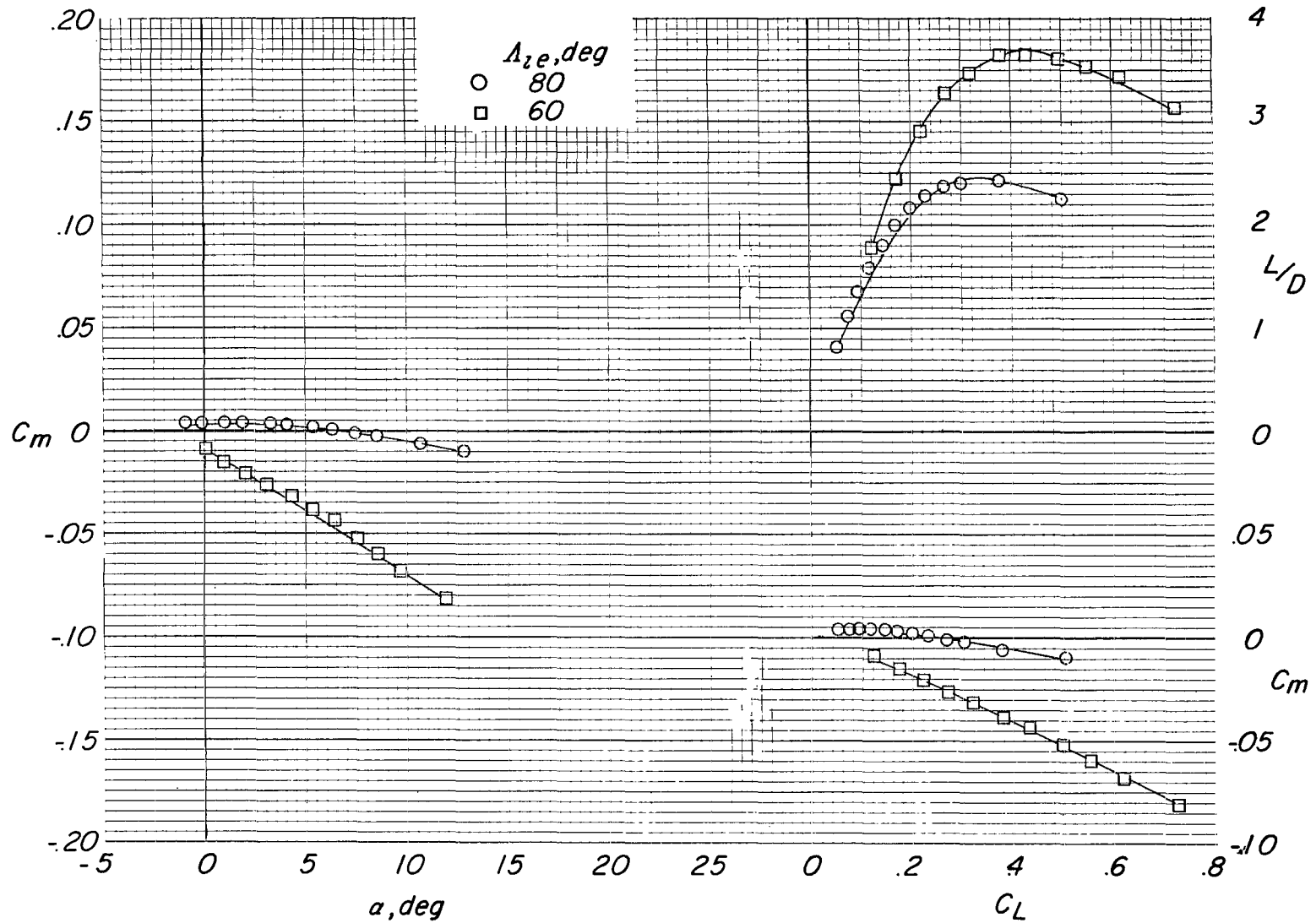

(e) M = 0.95. Concluded.

Figure 3.- Continued.

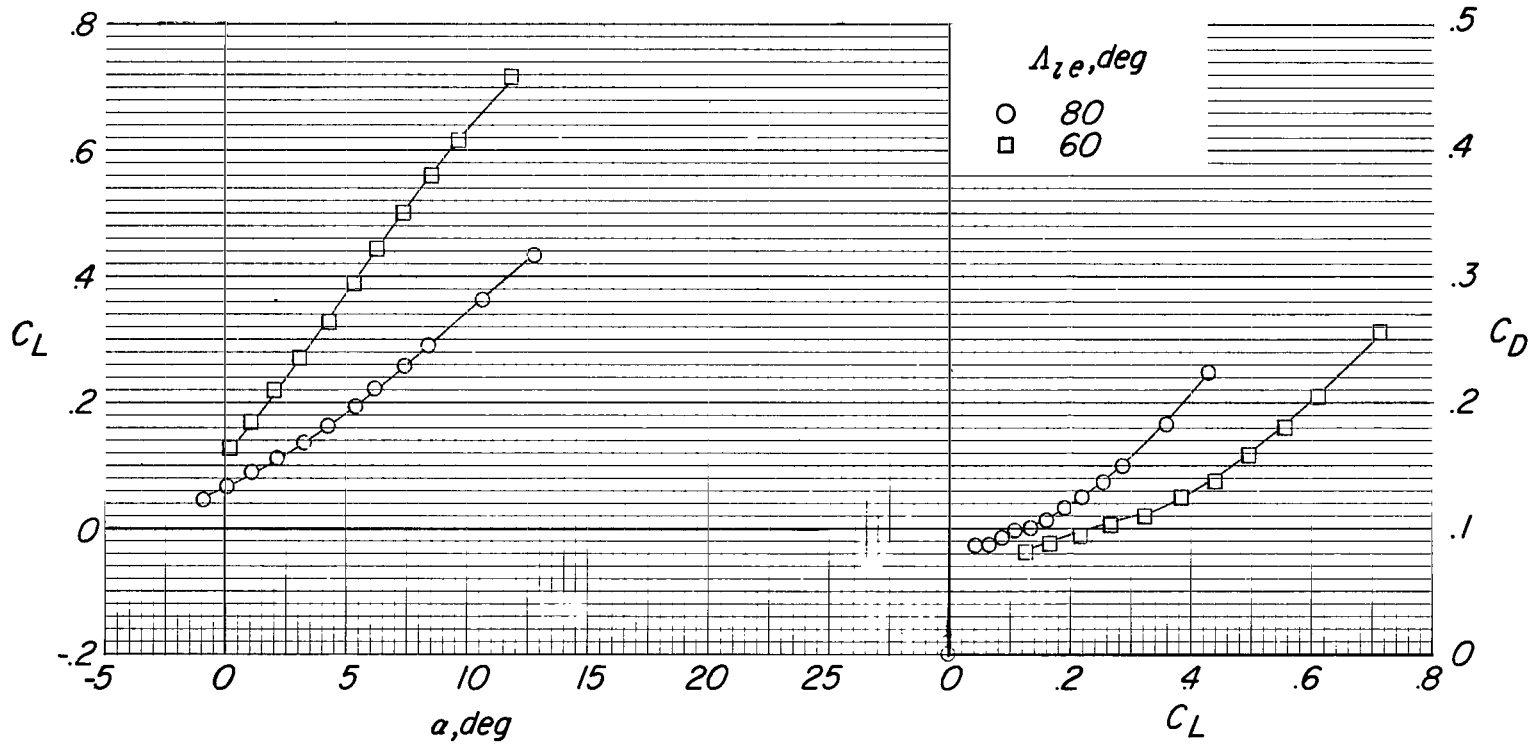

(f) M = 1.00.

Figure 3.- Continued.

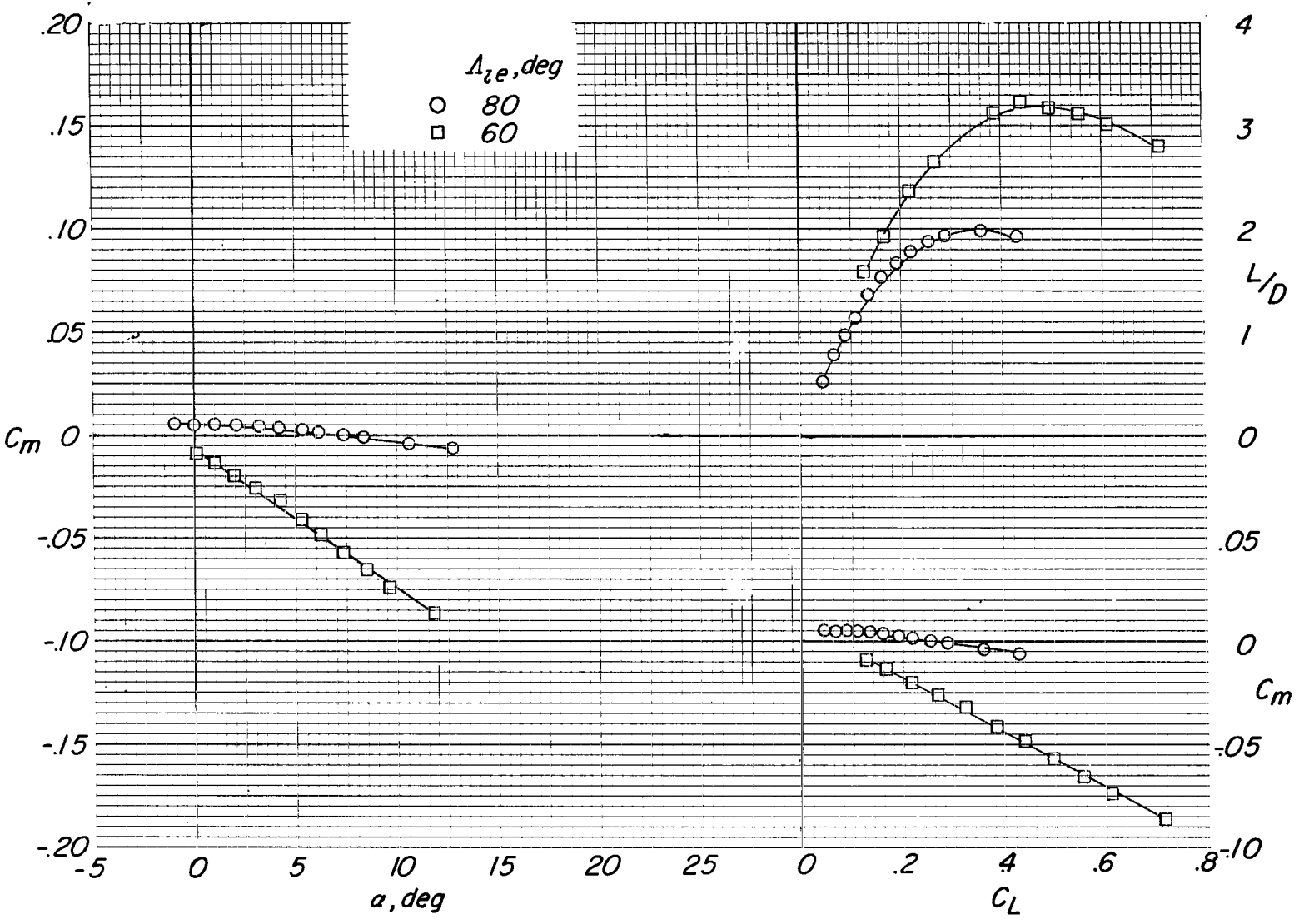

(f) M = 1.00. Concluded.

Figure 3.- Continued.

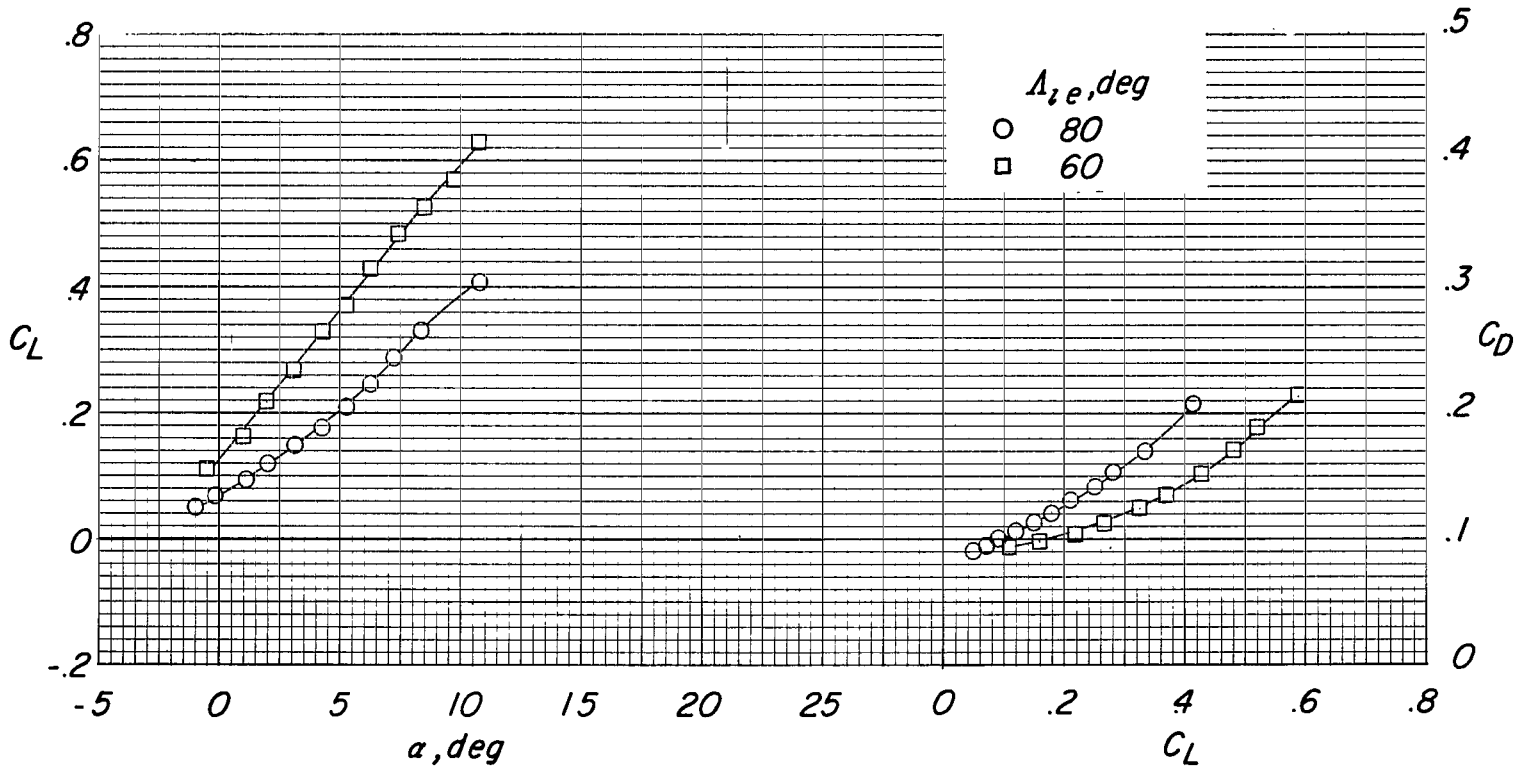

(g) M = 1.13.

Figure 3.- Continued.

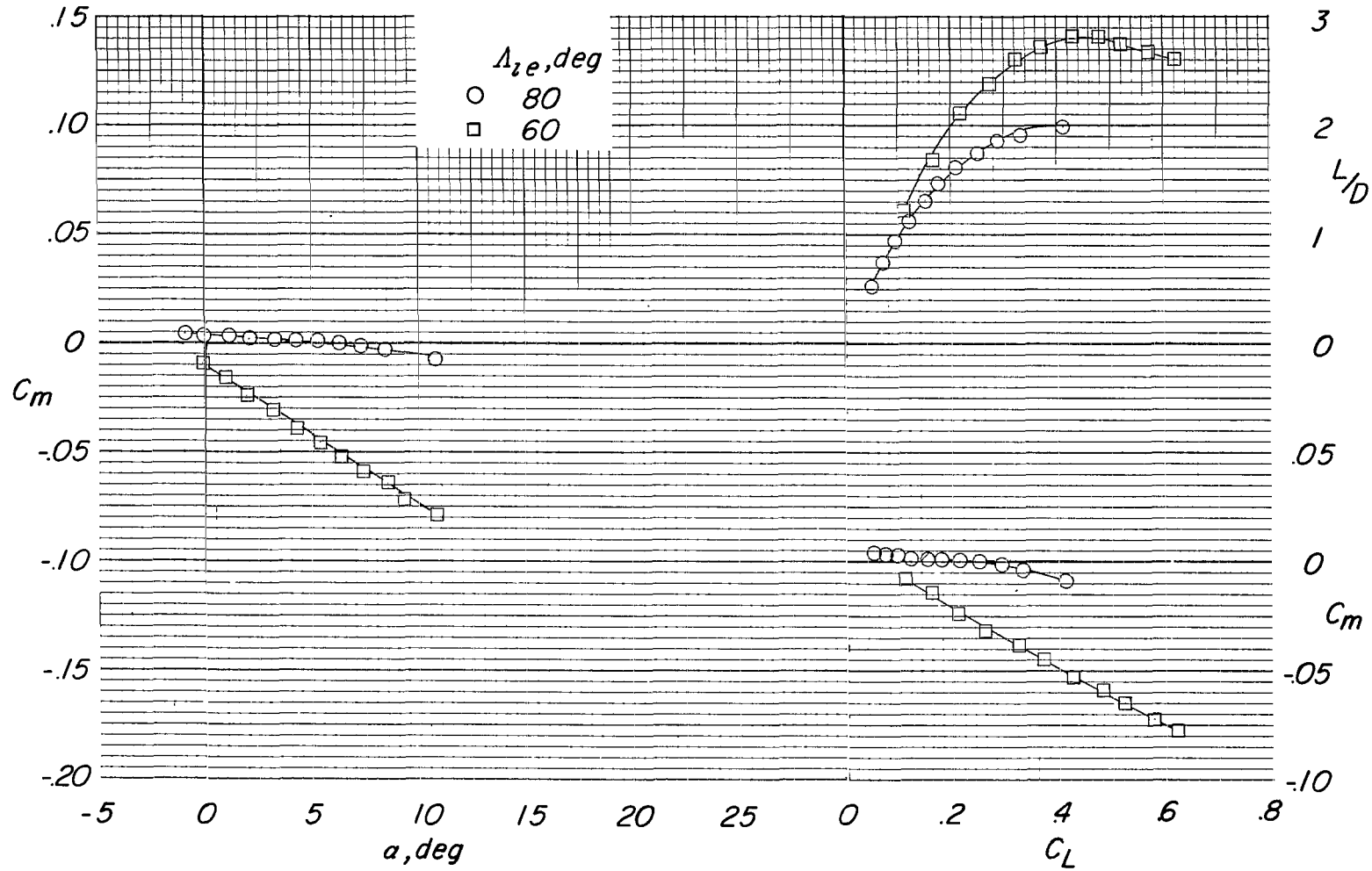

(g) M = 1.13. Concluded.

Figure 3.- Concluded.

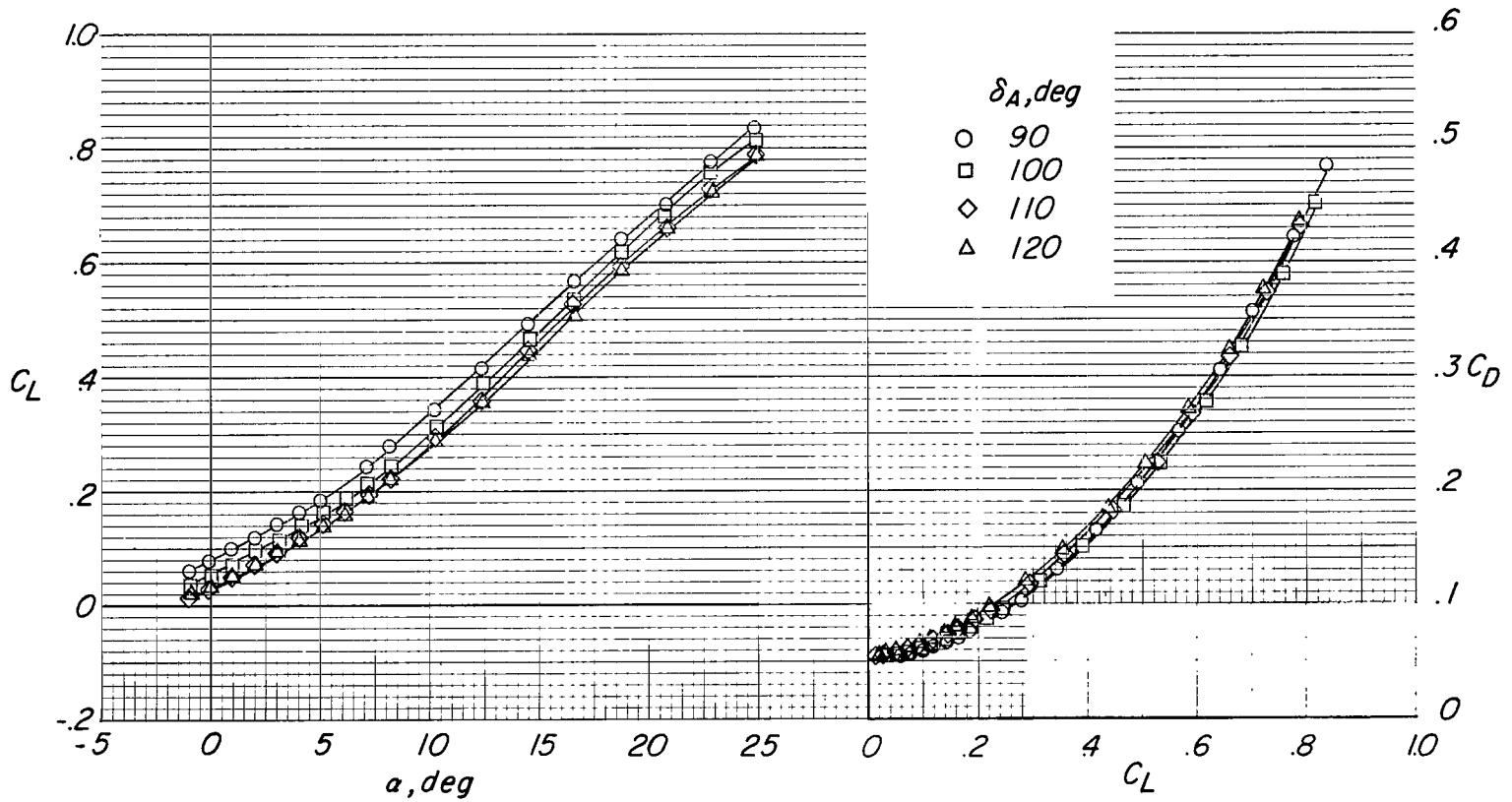

Figure 4.- Effects of afterbody flap deflection on longitudinal aerodynamic characteristics of configuration having wing leading edge swept back 80°. M = 0.40; trailing-edge flaps off; canard off.

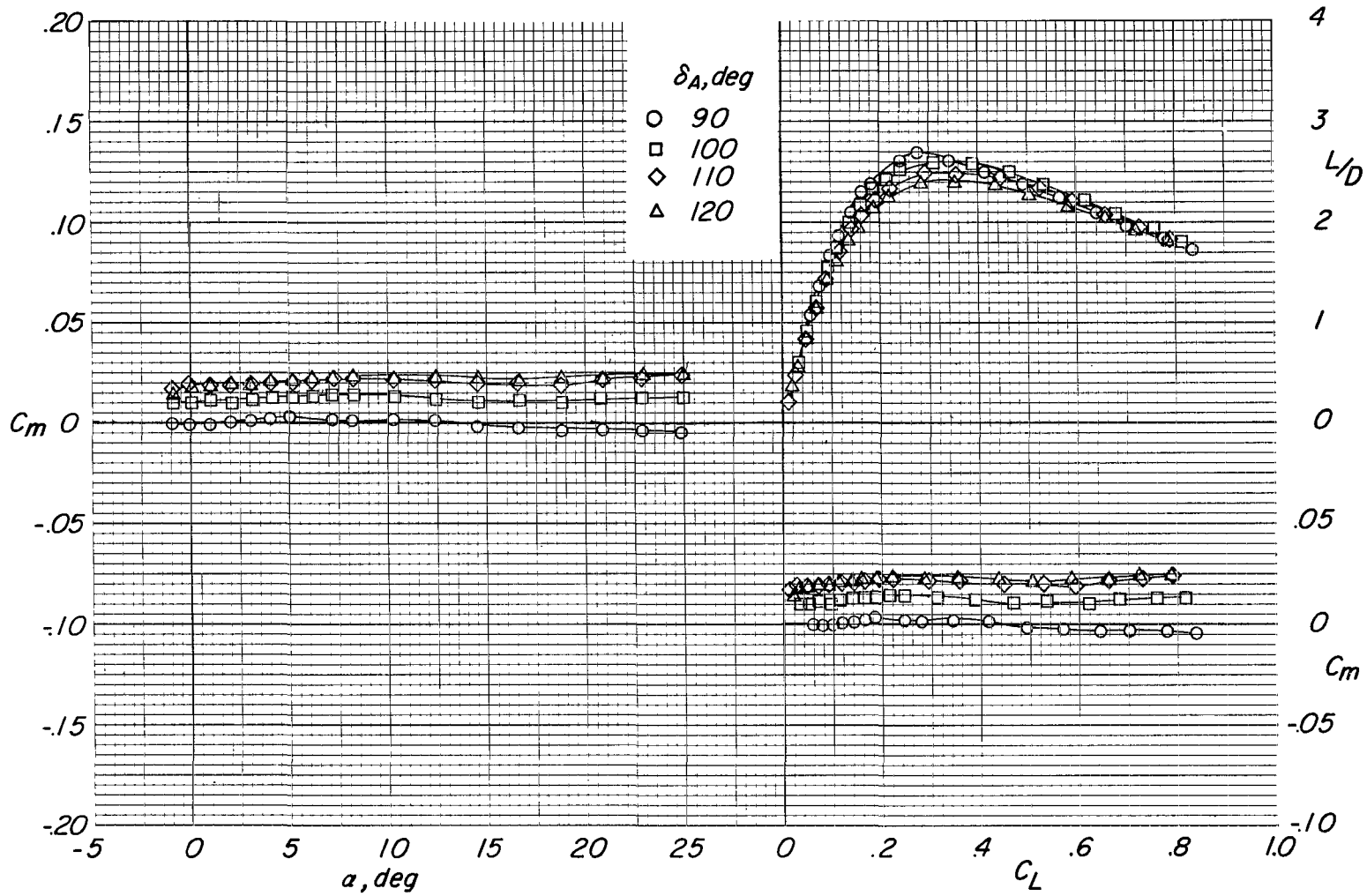

Figure 4.- Concluded.

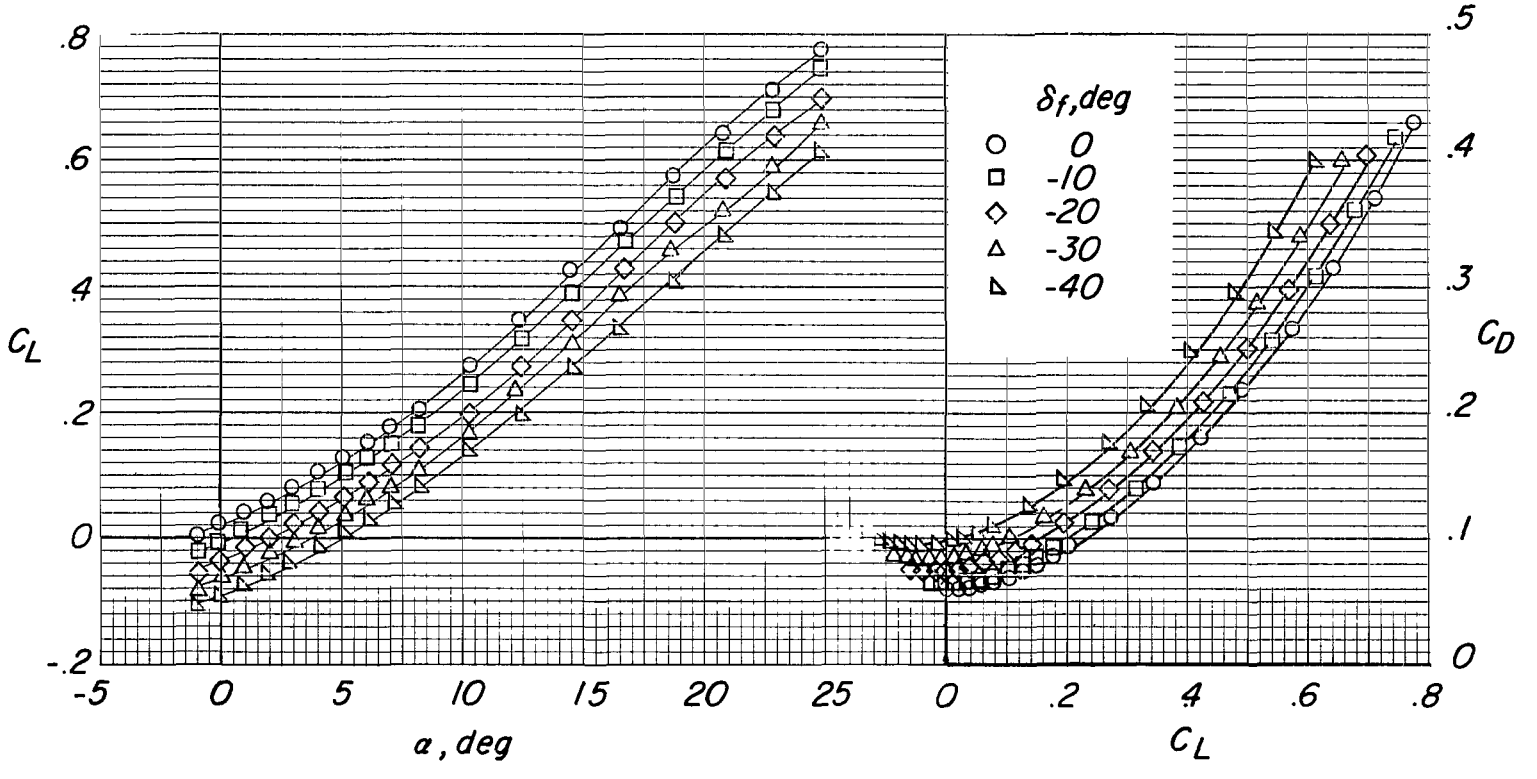

(a) $\Lambda_{le} = 80^\circ$.

Figure 5.- Effects of body trailing-edge flap deflection on longitudinal aerodynamic characteristics of configuration having afterbody flaps on, and various wing-panel sweeps. $M = 0.40$; $\delta_A = 120^\circ$; canard off.

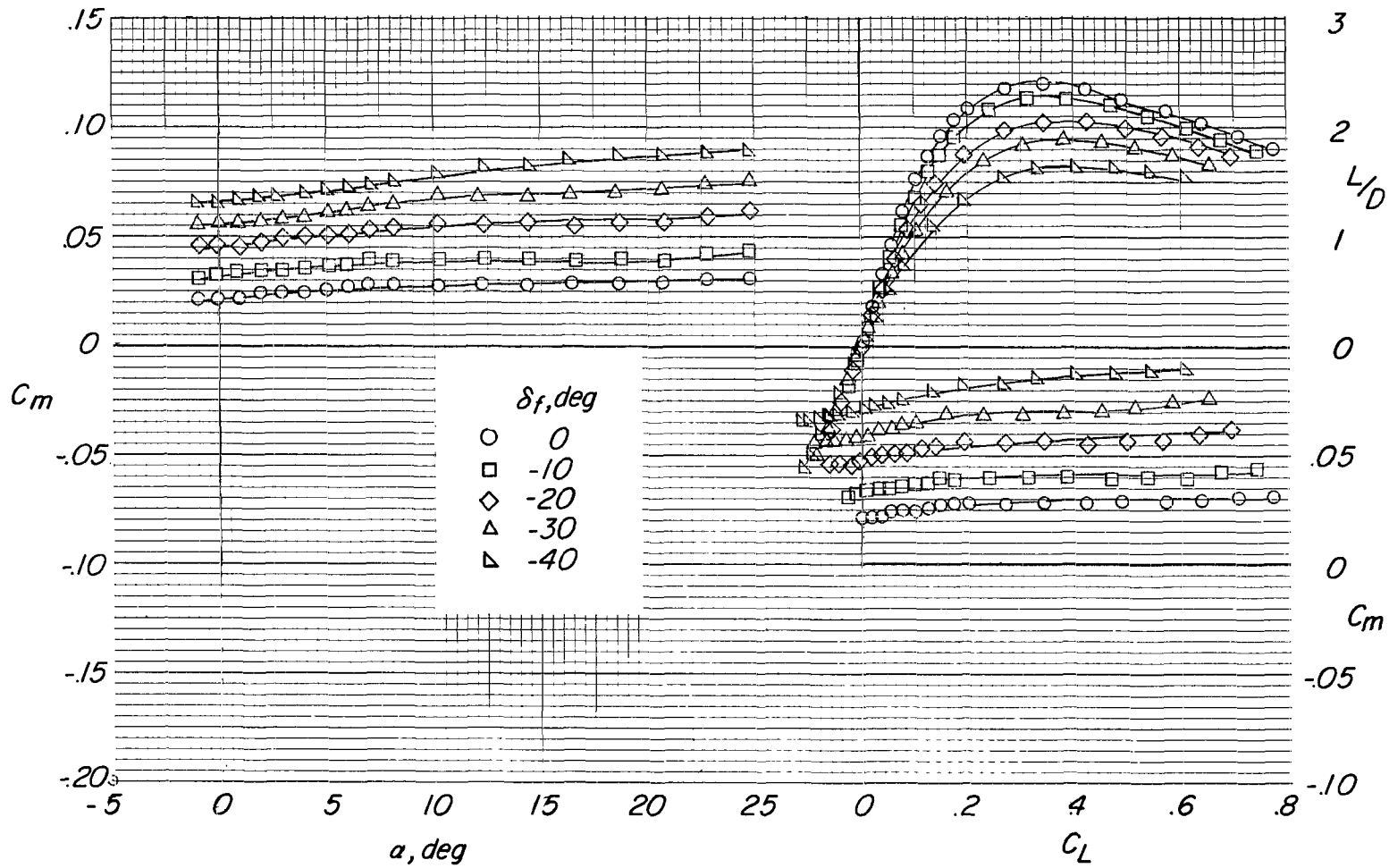

(a) $\Lambda_{le} = 80^\circ$. Concluded.

Figure 5.- Continued.

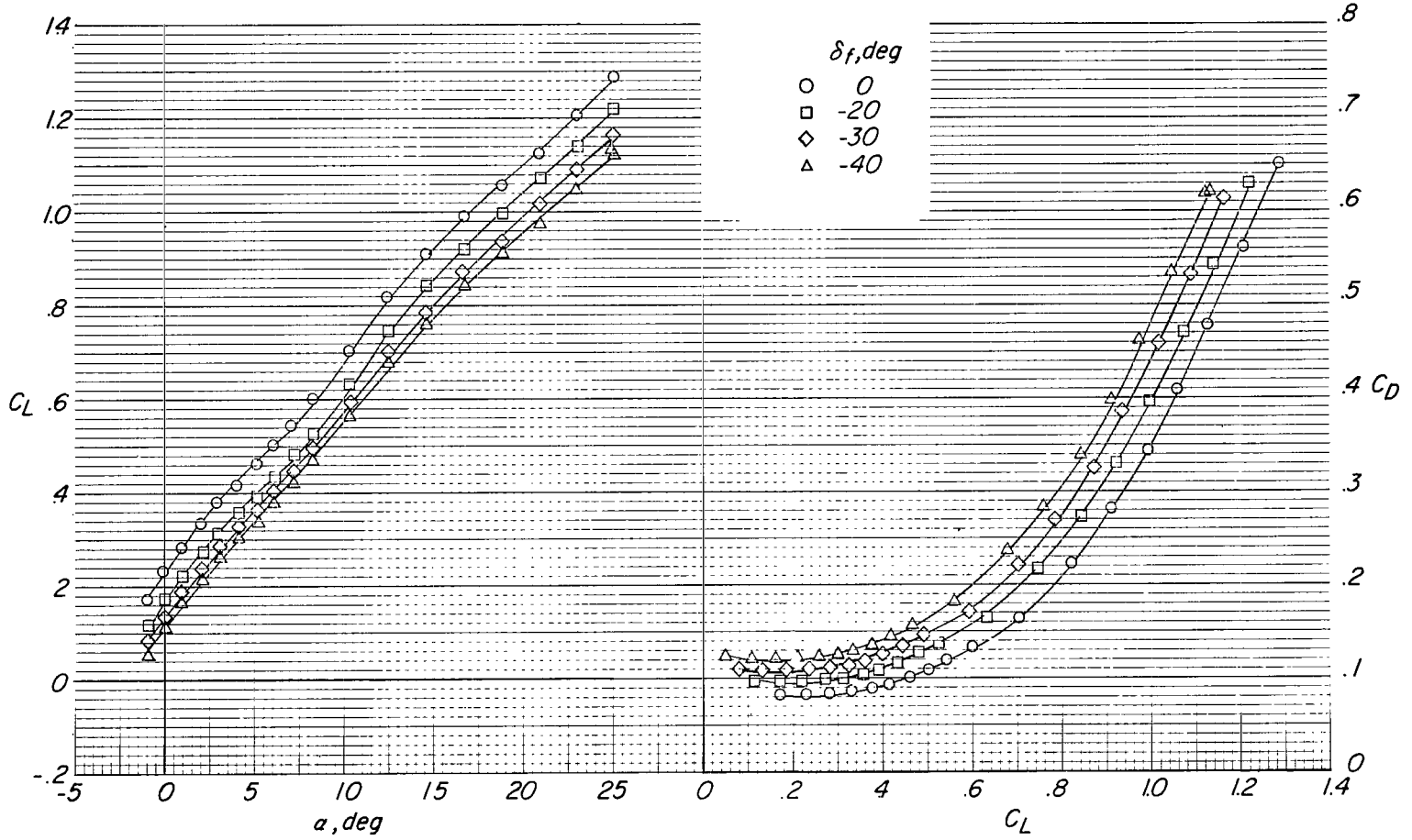

(b) $\Lambda_{le} = 40^{\circ}$.

Figure 5.- Continued.

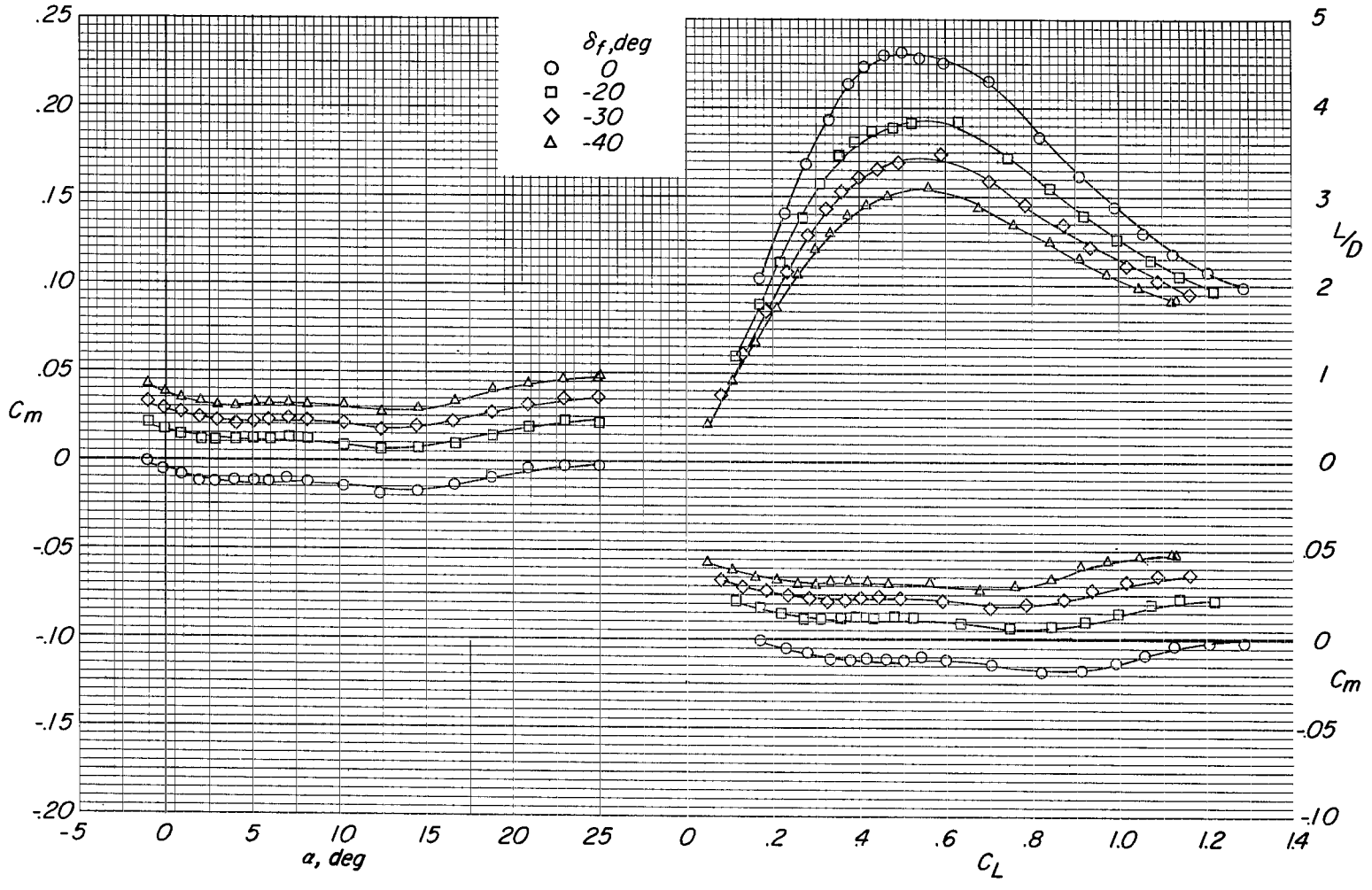

(b) $\Lambda_{le} = 40^{\circ}$. Concluded.

Figure 5.- Continued.

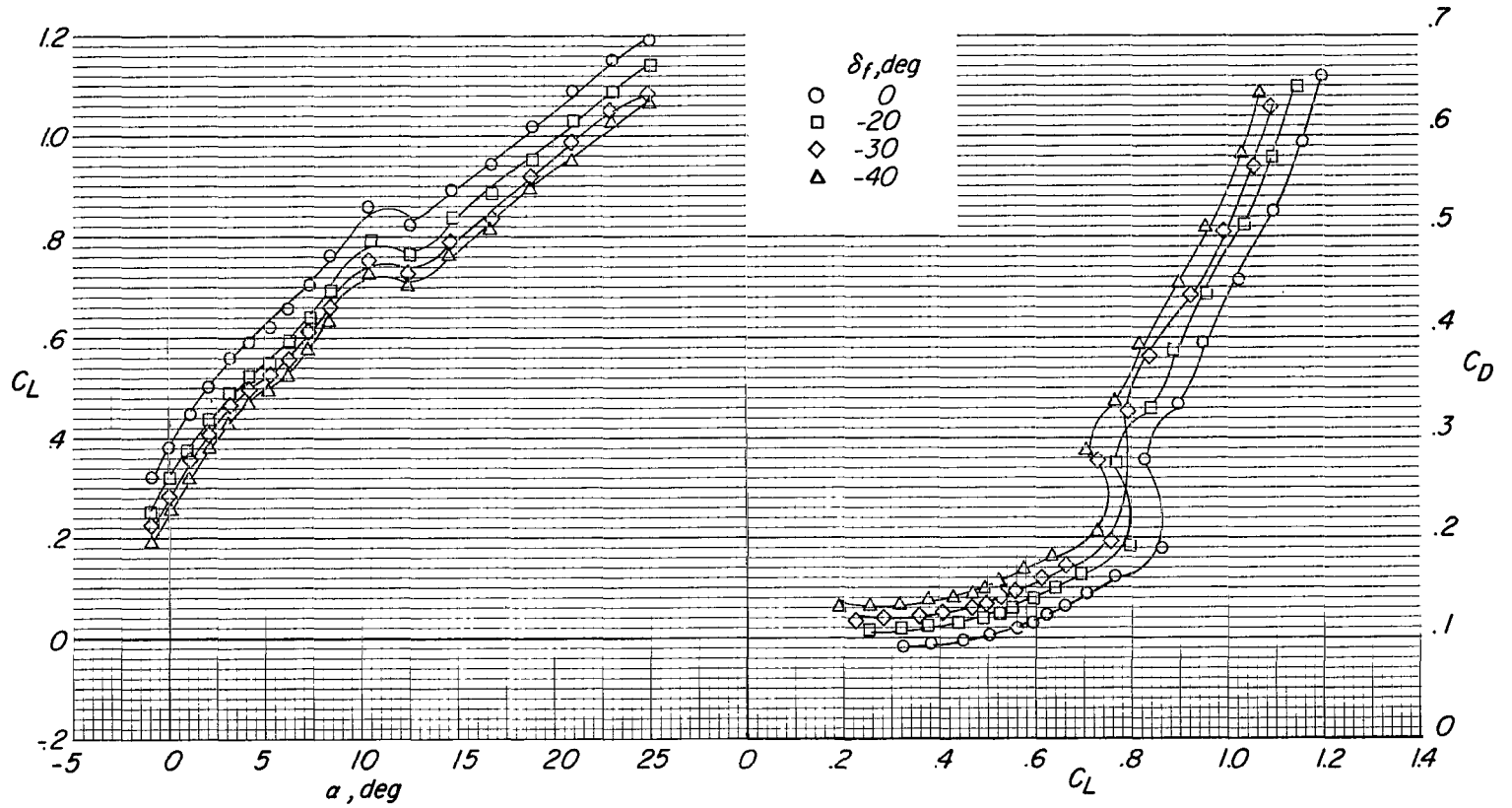

(c) $\Lambda_{le} = 20^{\circ}$.

Figure 5.- Continued.

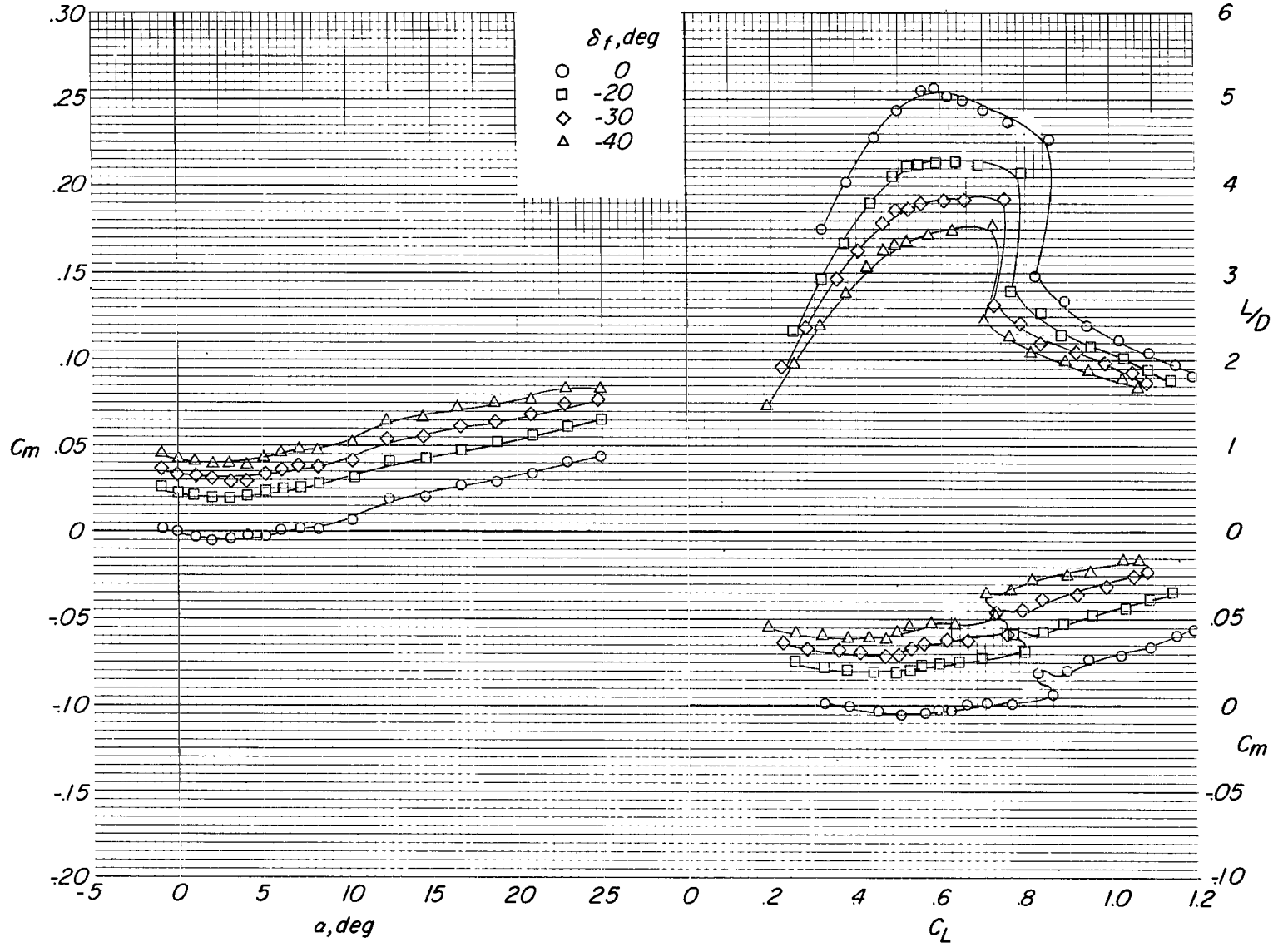

(c) $\Lambda_{le} = 20^\circ$. Concluded.

Figure 5.- Continued.

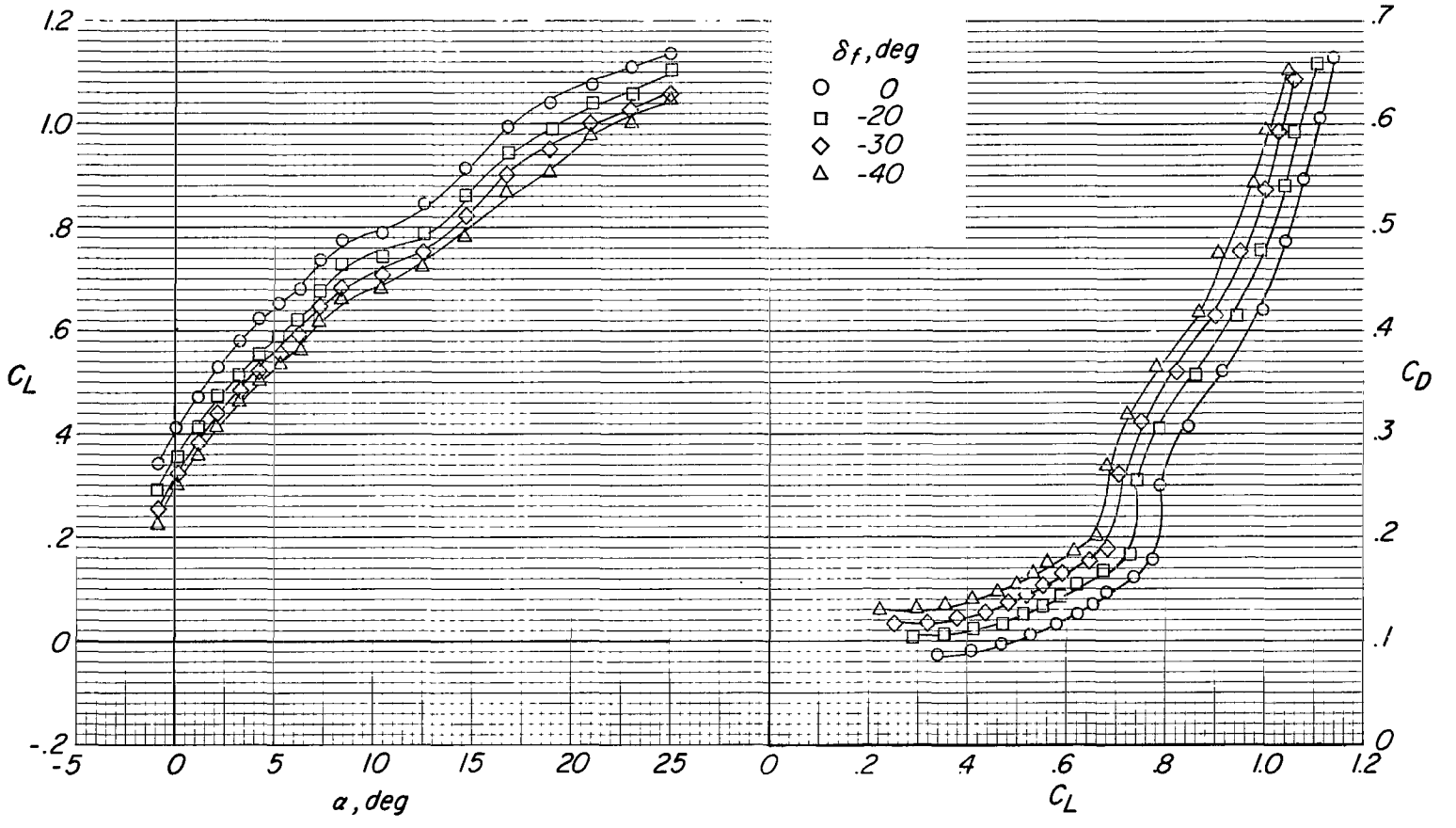

(d) $\Lambda_{le} = 0^\circ$.

Figure 5.- Continued.

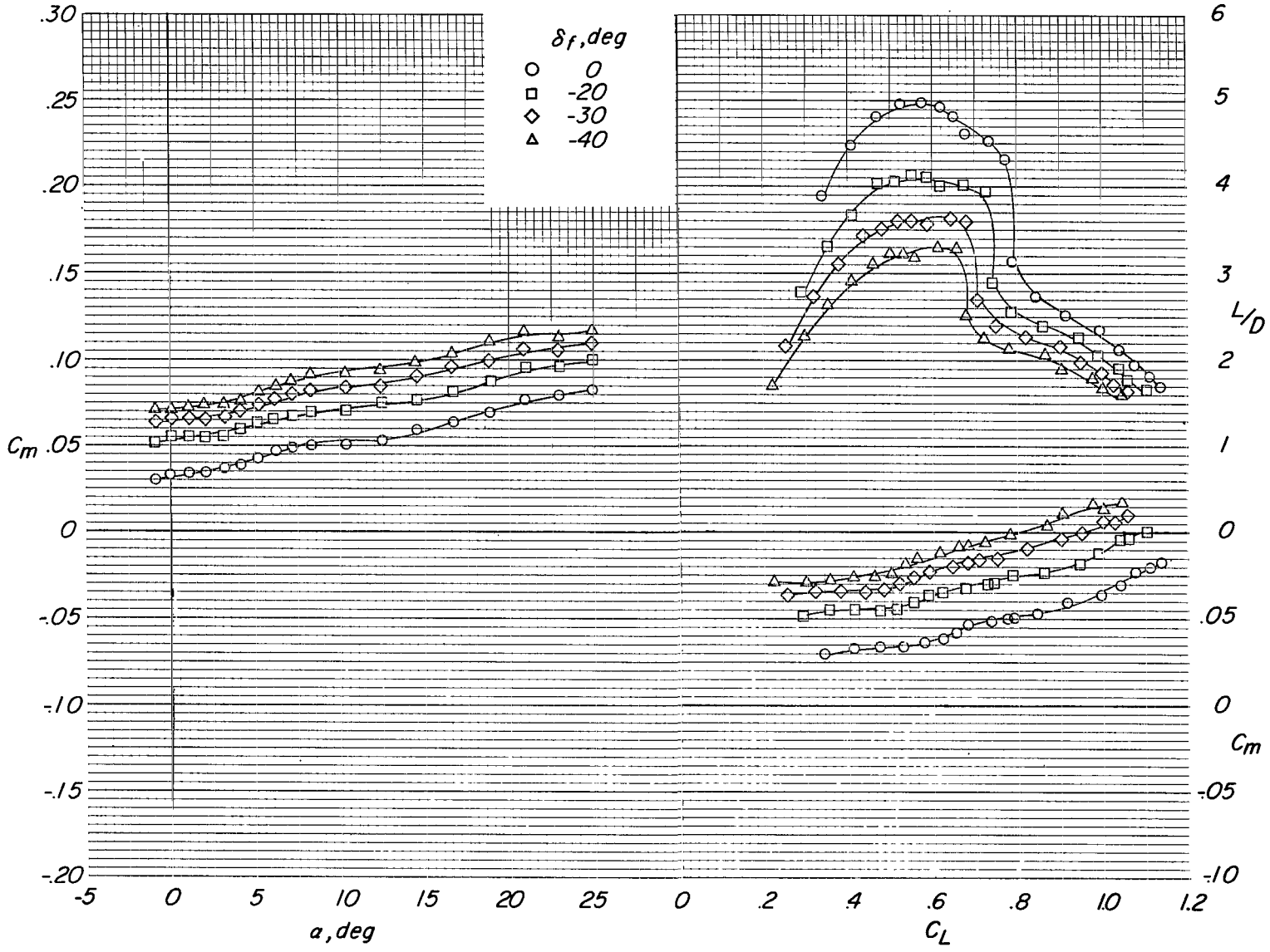

(d) $\Lambda_{le} = 0°$. Concluded.

Figure 5.- Concluded.

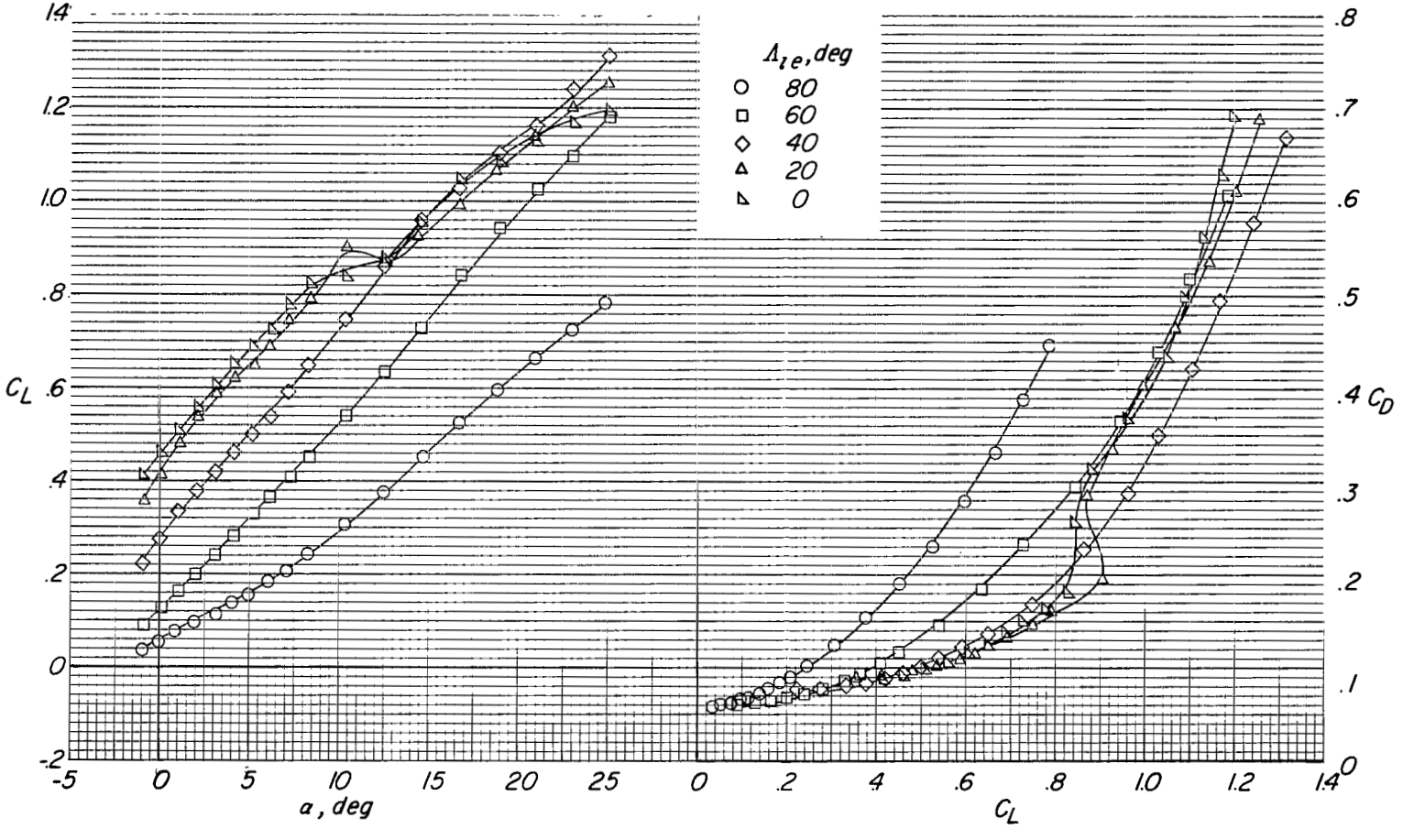

(a) $\delta_f = 0^\circ$.

Figure 6.- Effects of wing-panel sweep on longitudinal aerodynamic characteristics of configuration with body trailing-edge flap on. M = 0.40; afterbody flaps off; canard off.

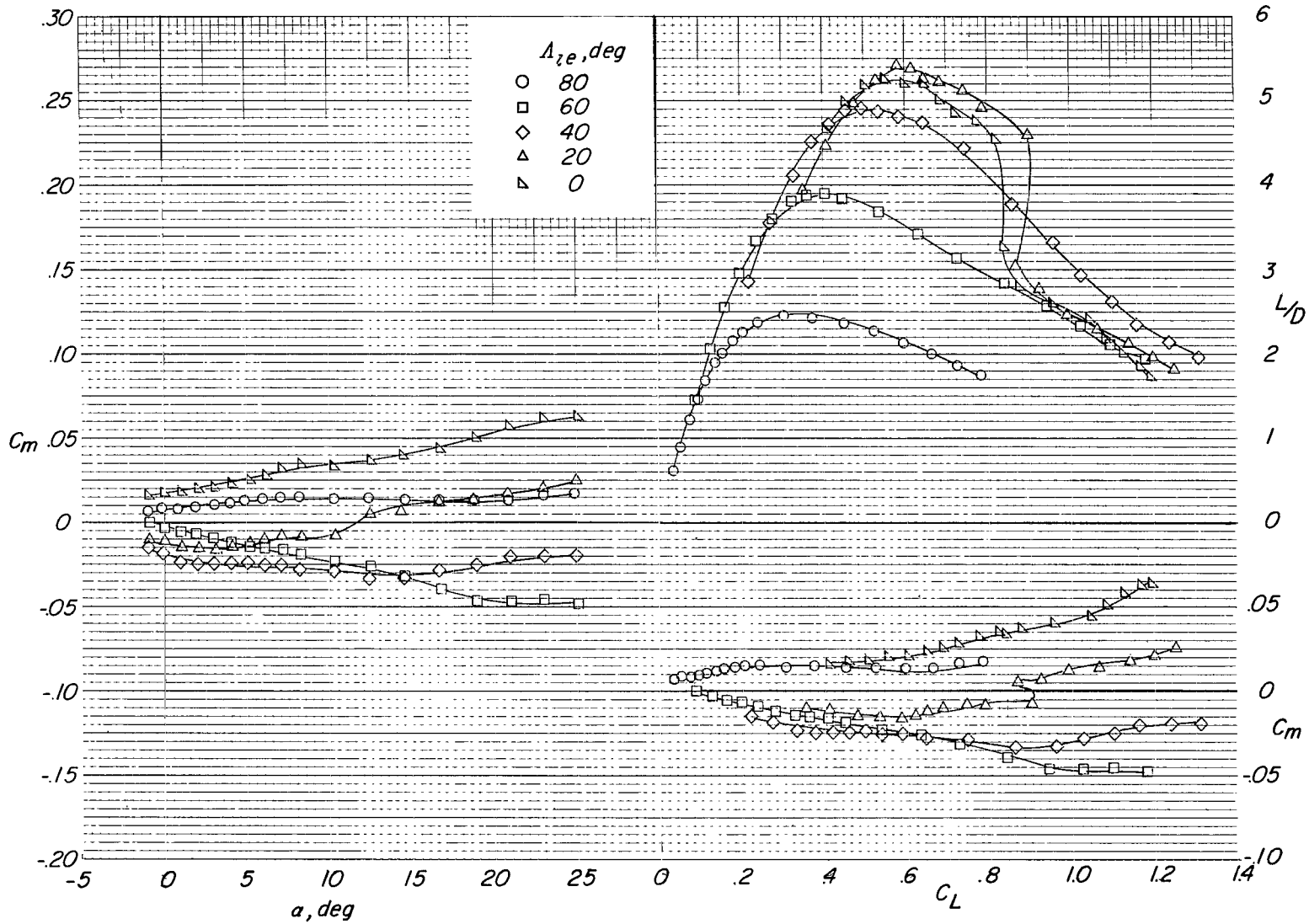

(a) $\delta_f = 0^\circ$. Concluded.

Figure 6.- Continued.

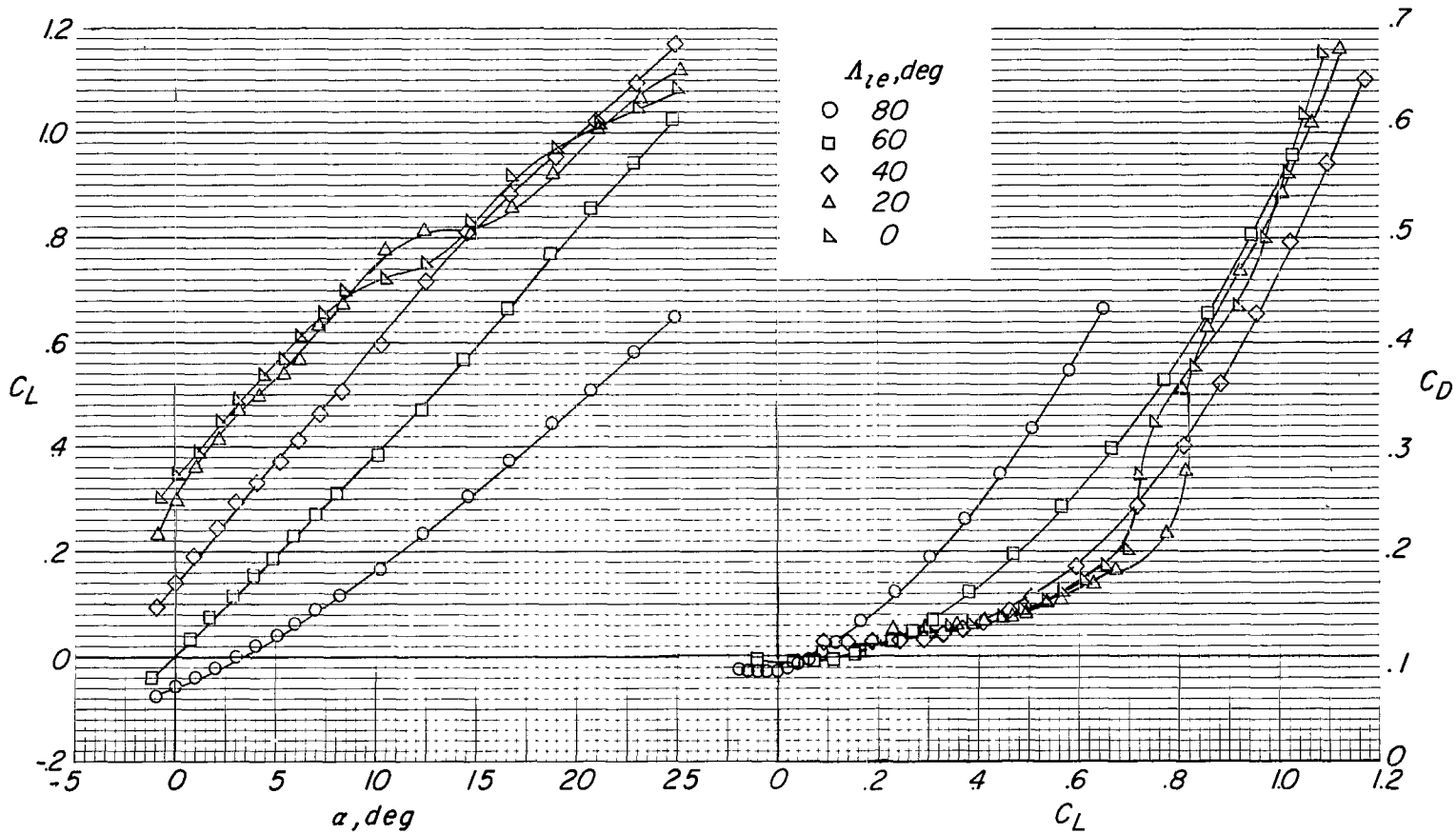

(b) $\delta_f = 40^\circ$.

Figure 6.- Continued.

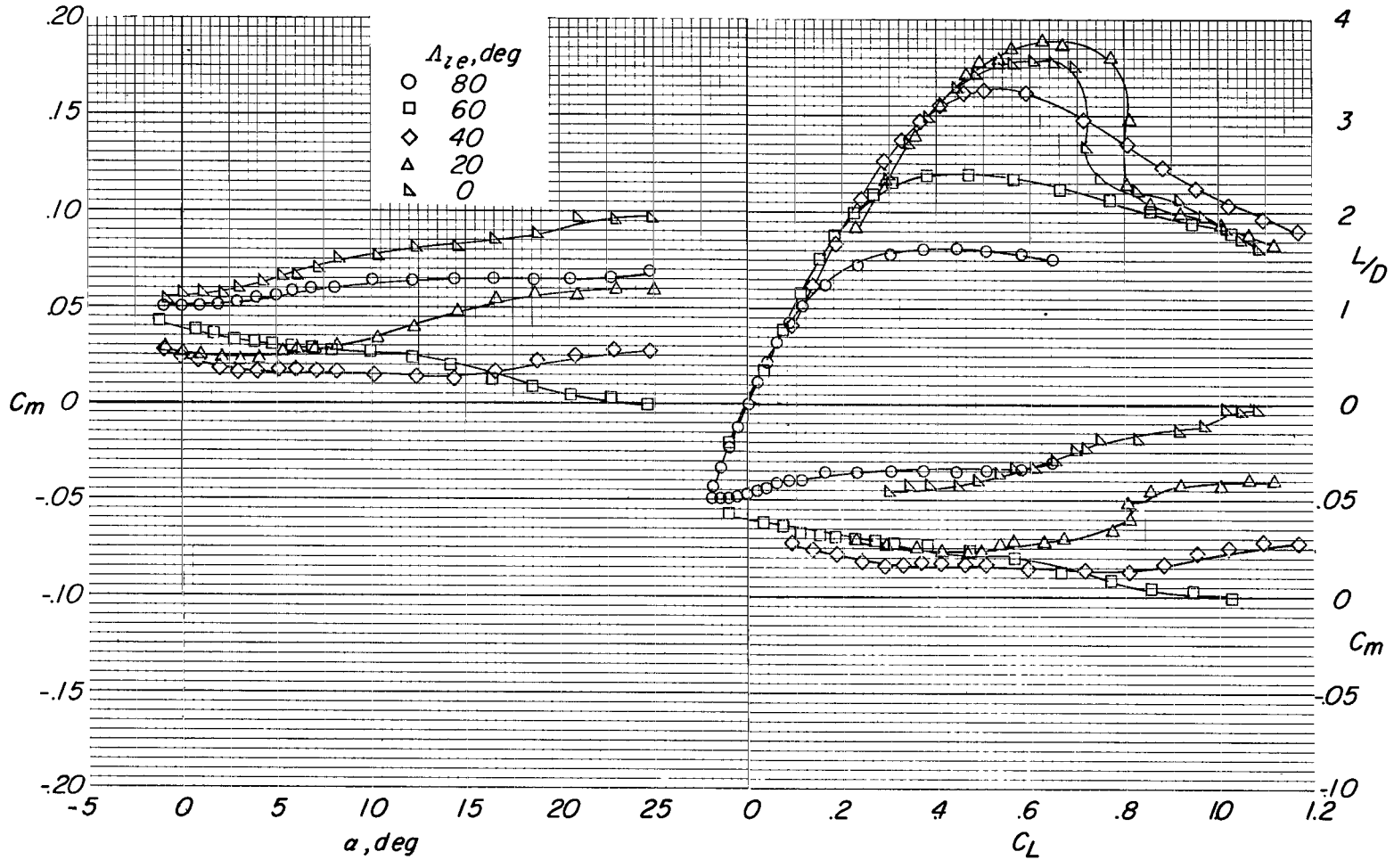

(b) $\delta_f = 40^\circ$. Concluded.

Figure 6.- Concluded.

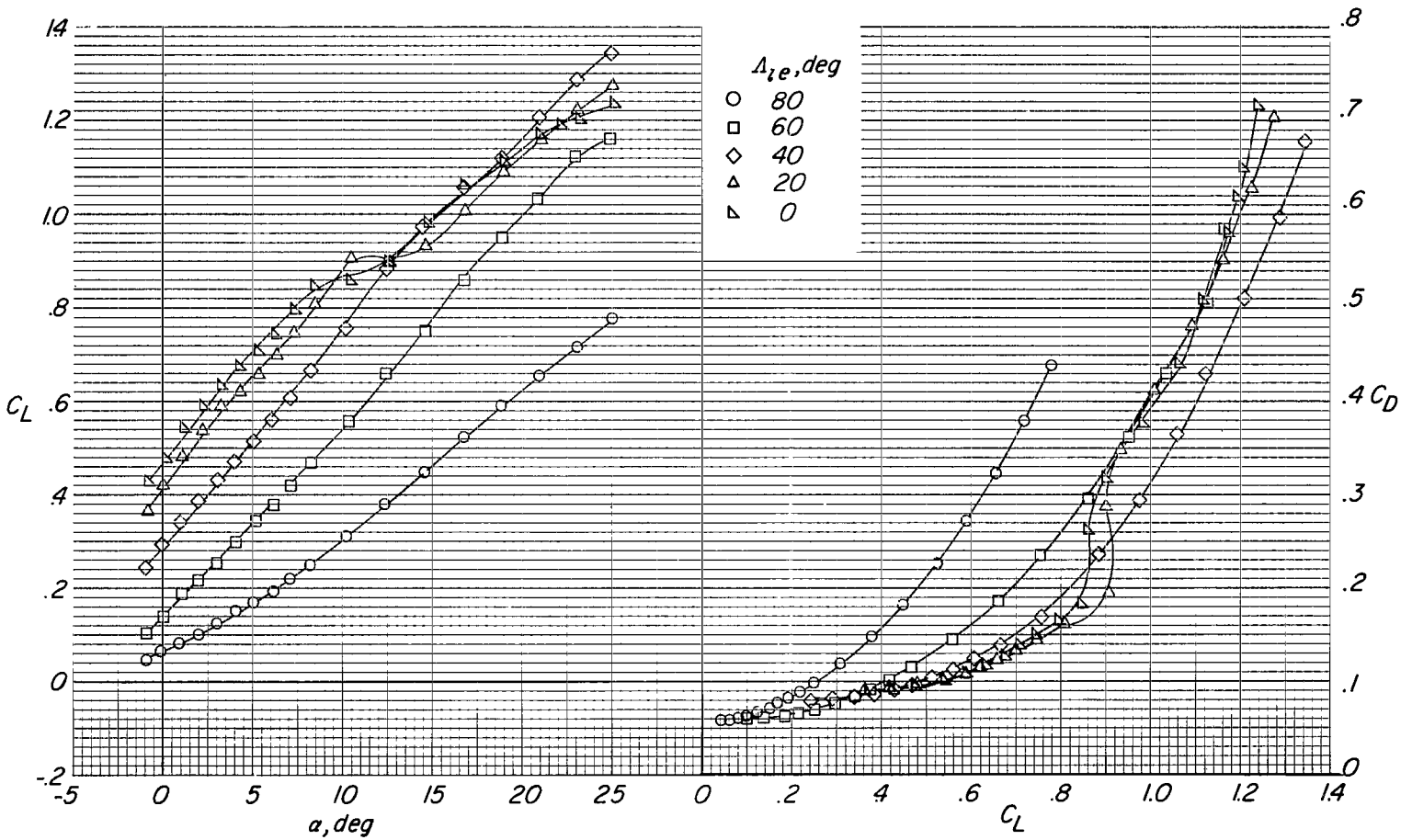

(a) Canard leading- and trailing-edge flaps undeflected.

Figure 7.- Effects of wing-panel sweep on longitudinal aerodynamic characteristics of configuration with canard on. M = 0.40; trailing-edge and afterbody flaps off.

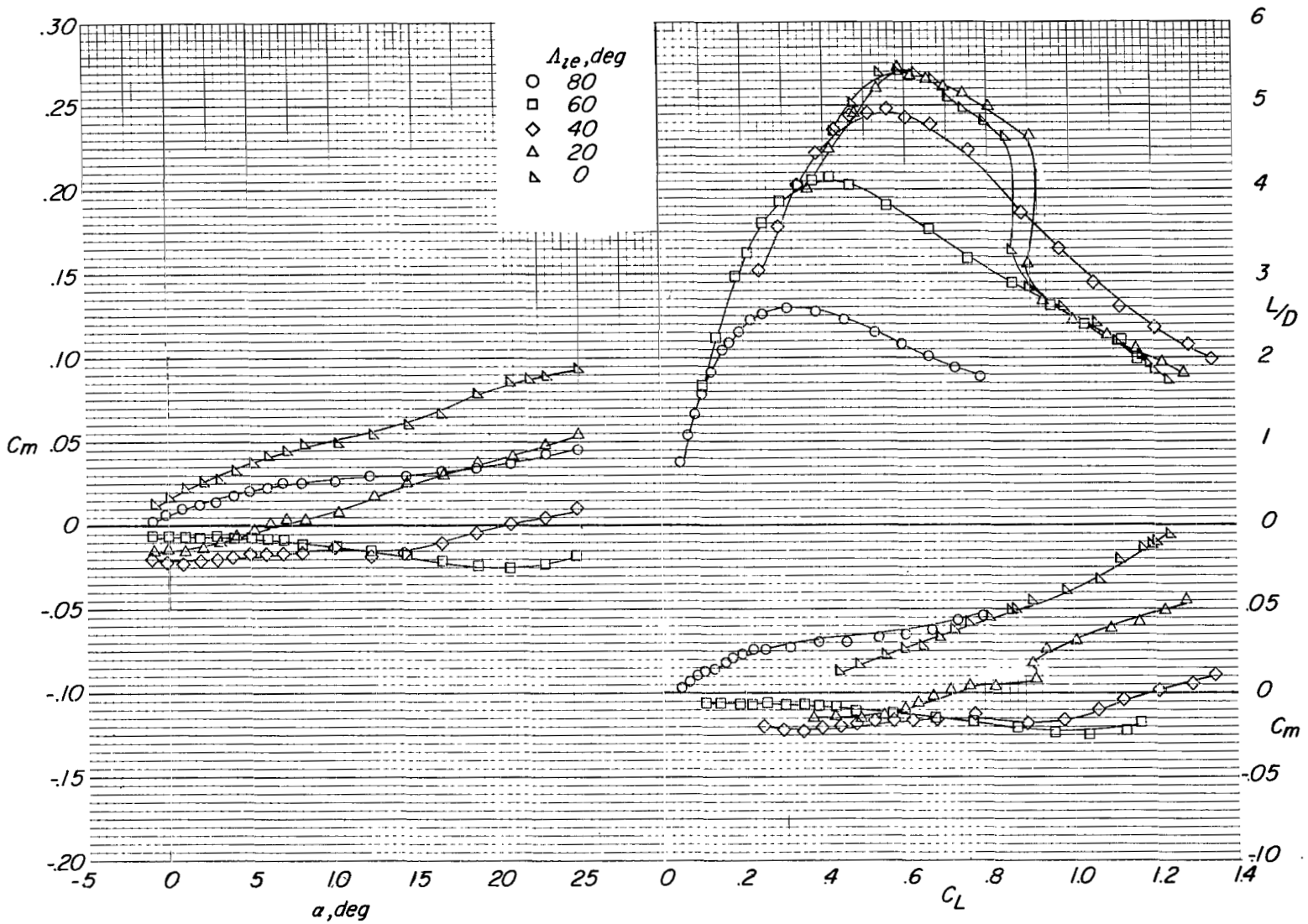

(a) Canard leading- and trailing-edge flaps undeflected. Concluded.

Figure 7.- Continued.

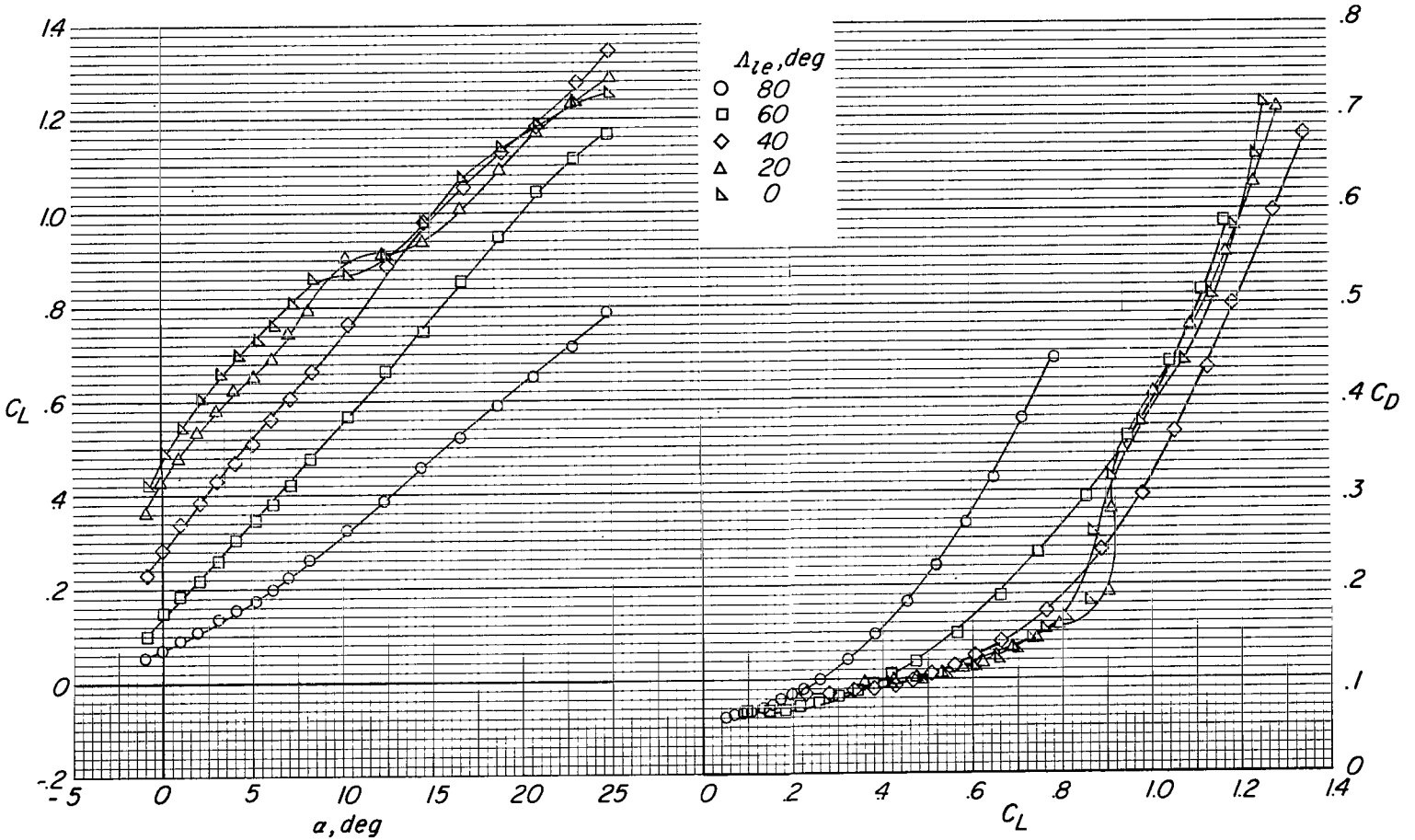

(b) Canard flaps deflected: $\delta_{f,c} = 30^{\circ}$, $\delta_{n,c} = -20^{\circ}$.

Figure 7.- Continued.

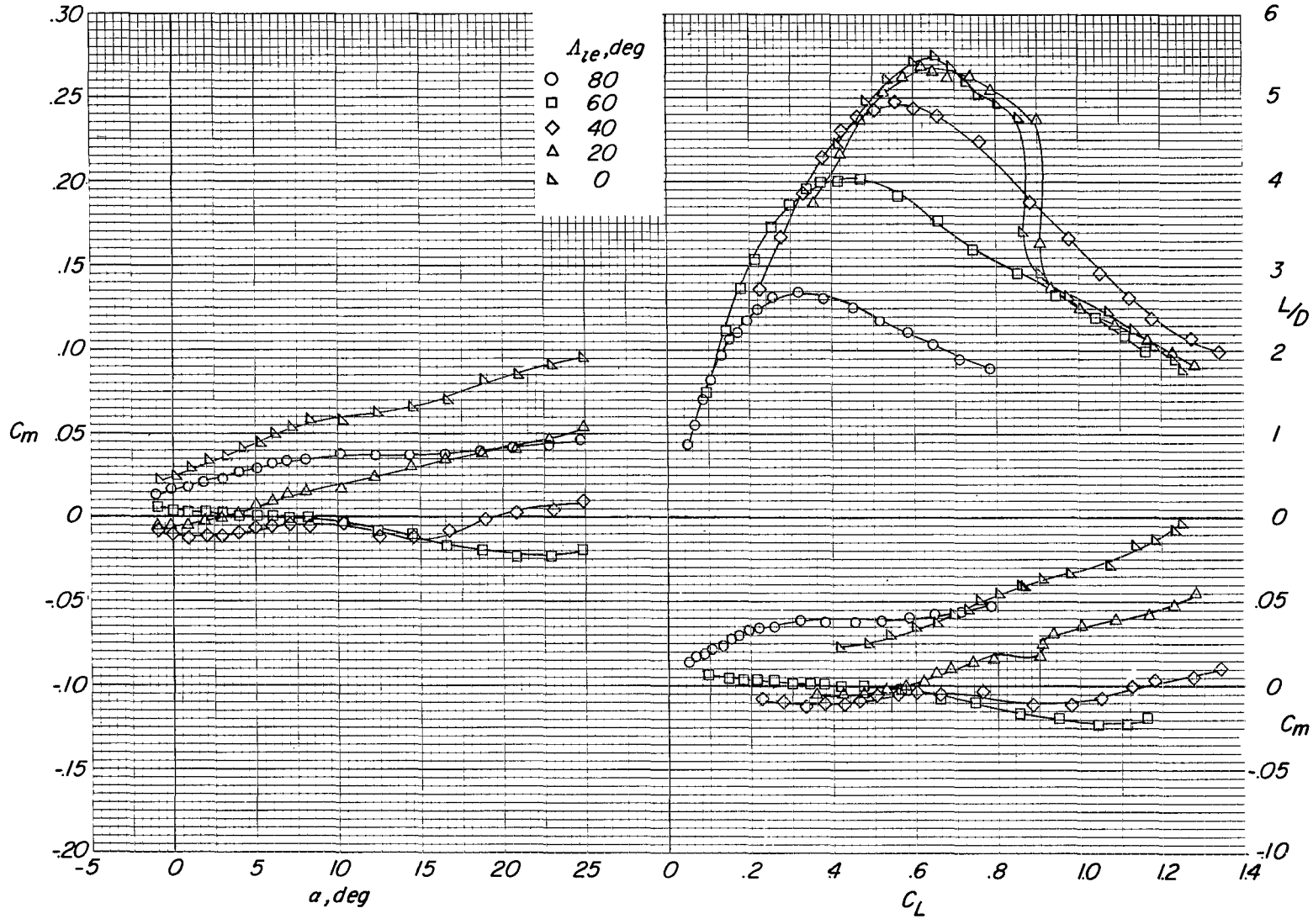

(b) Canard flaps deflected: $\delta_{f,c} = 30°$, $\delta_{n,c} = -20°$. Concluded.

Figure 7.- Concluded.

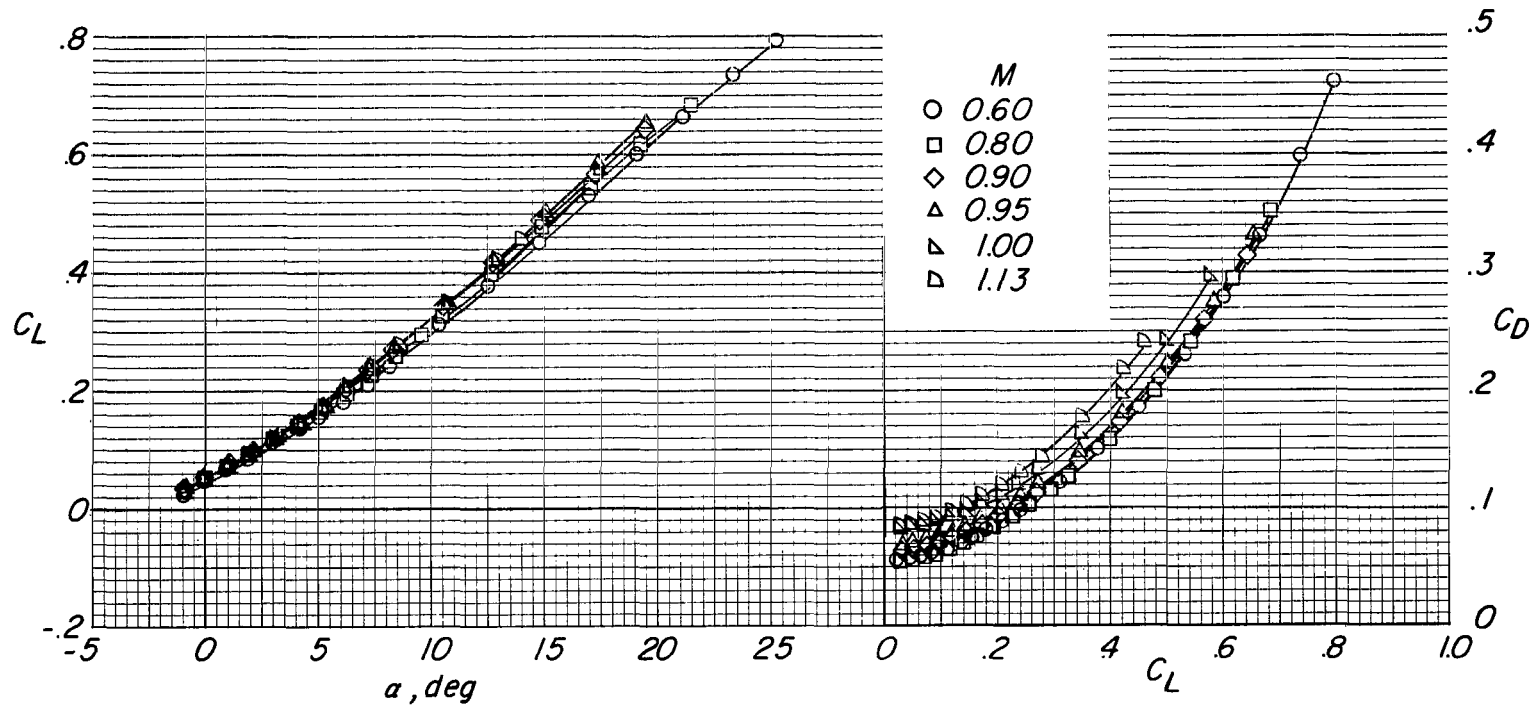

(a) $\delta_f = 0^\circ$.

Figure 8.- Effects of increasing Mach number on longitudinal aerodynamic characteristics of configuration having wing panels swept back 80° with afterbody flaps deflected 100°. Canard off.

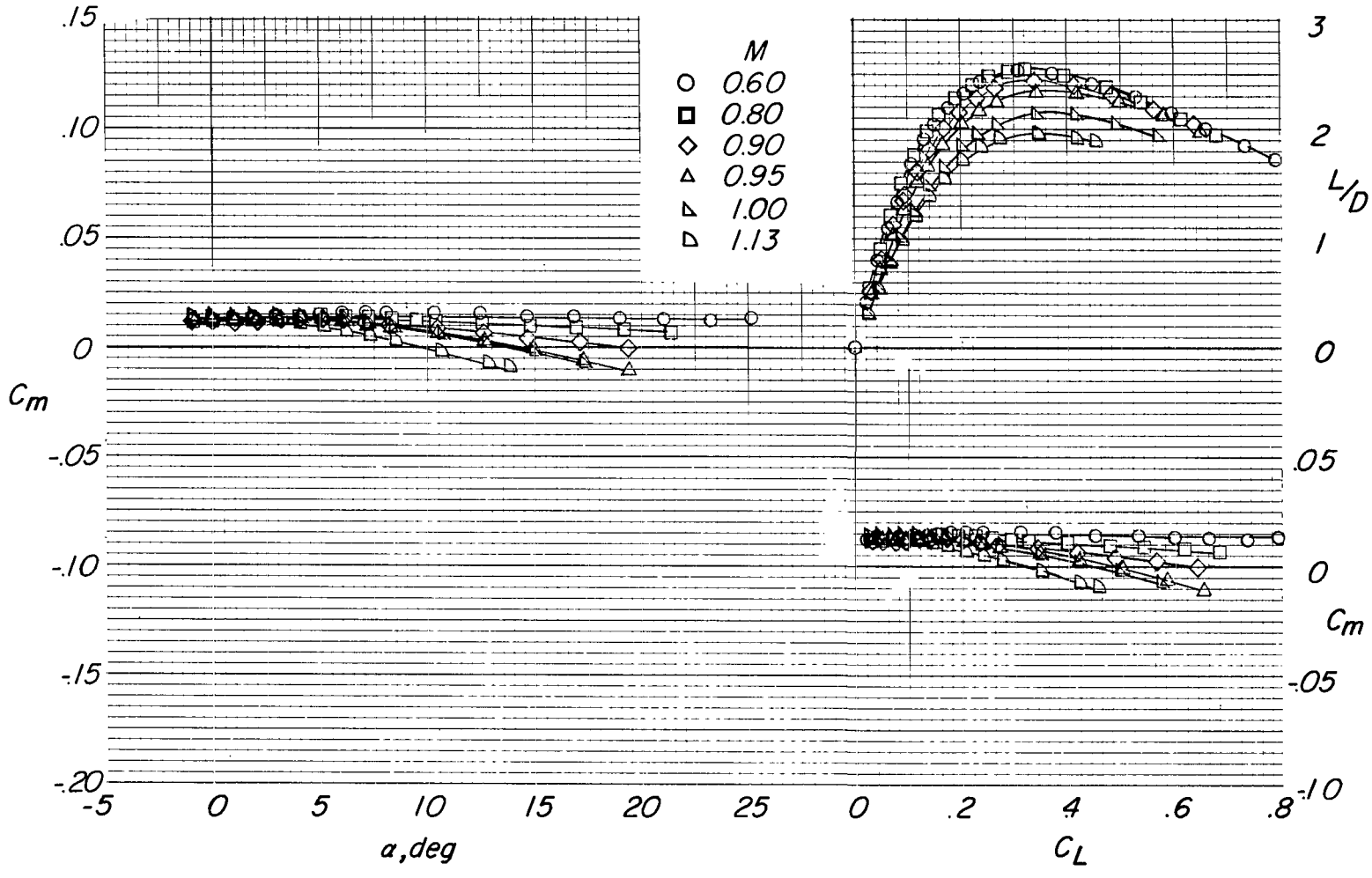

(a) $\delta_f = 0^\circ$. Concluded.

Figure 8.- Continued.

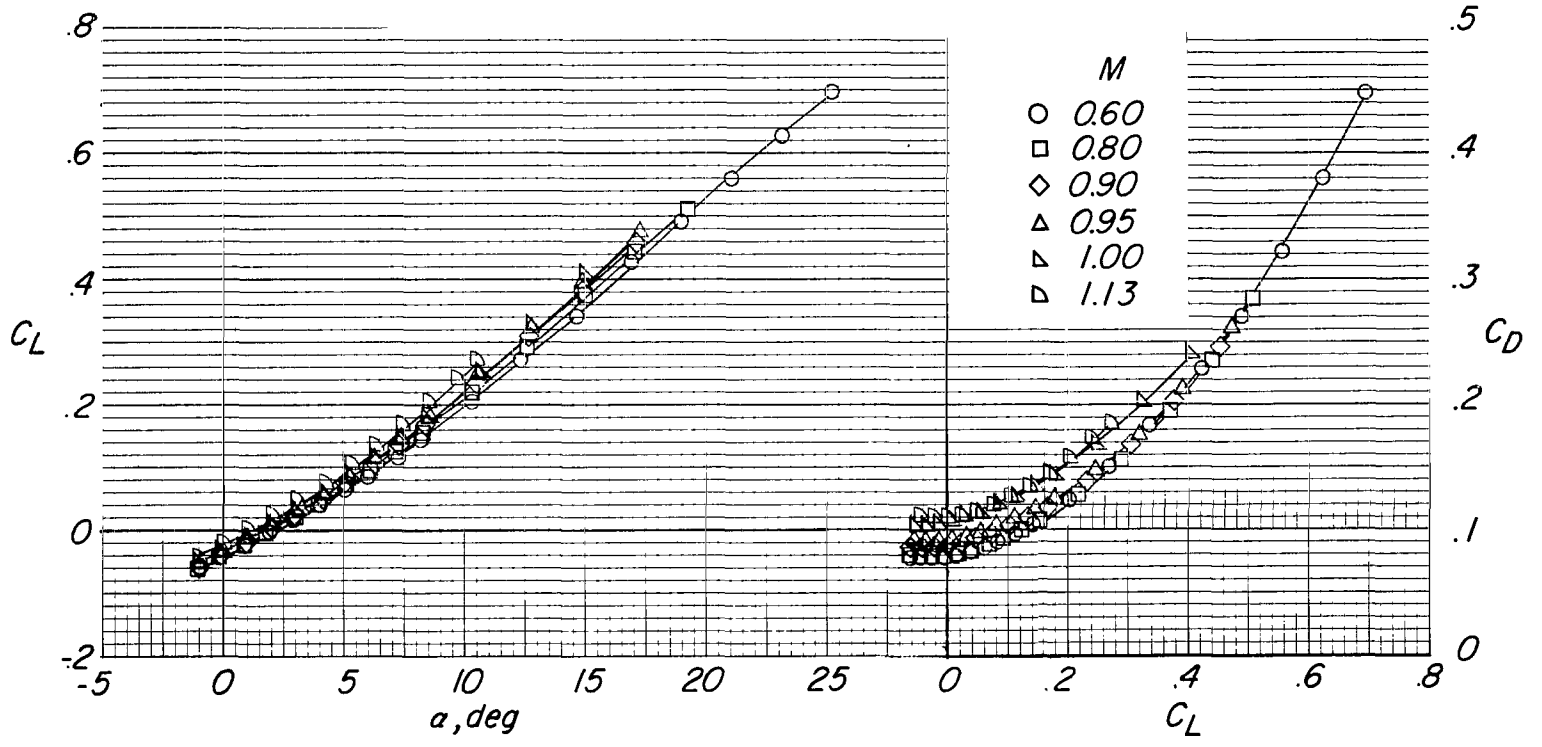

(b) $\delta_f = 40°$.

Figure 8.- Continued.

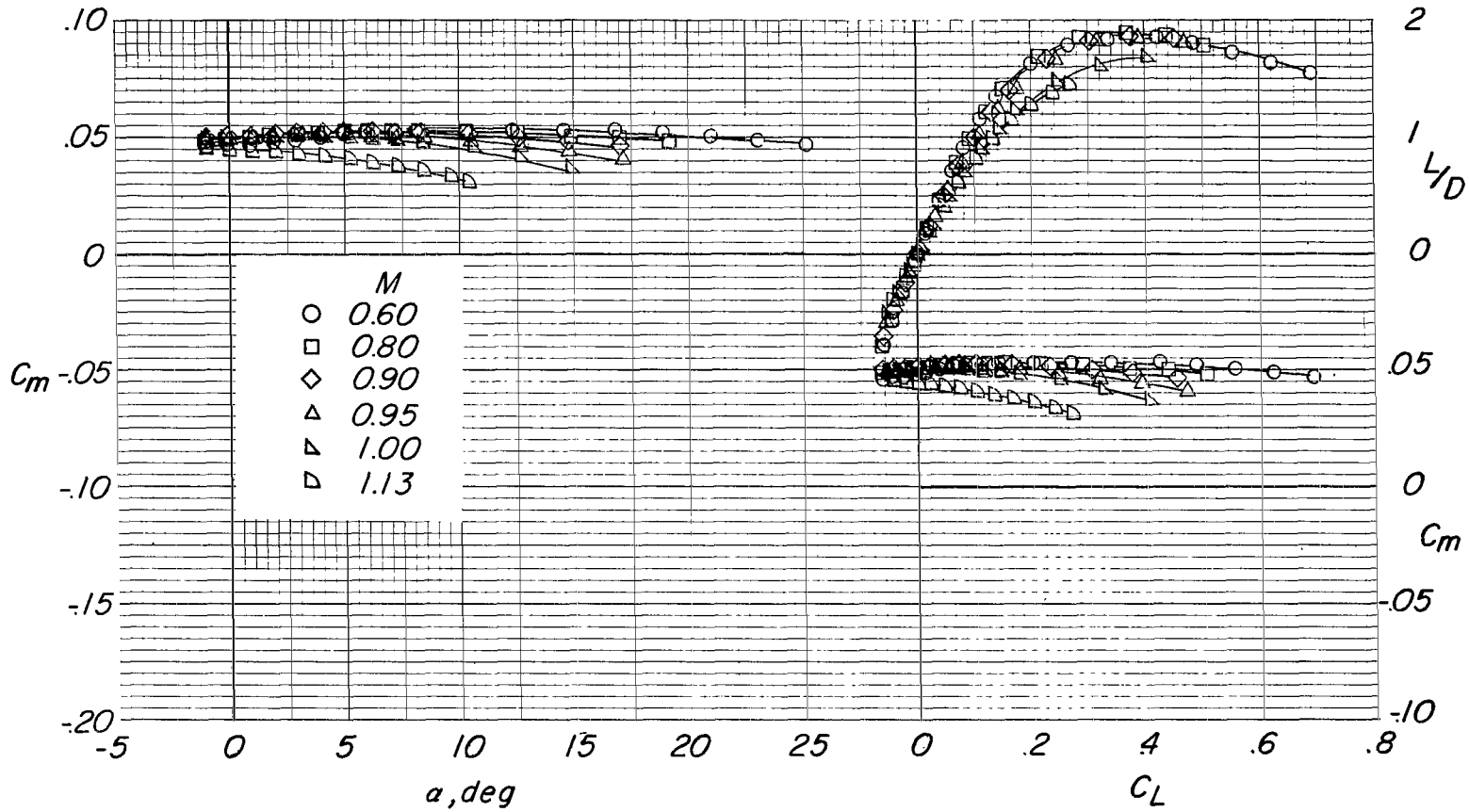

(b) $\delta_f = 40^\circ$. Concluded.

Figure 8.- Concluded.

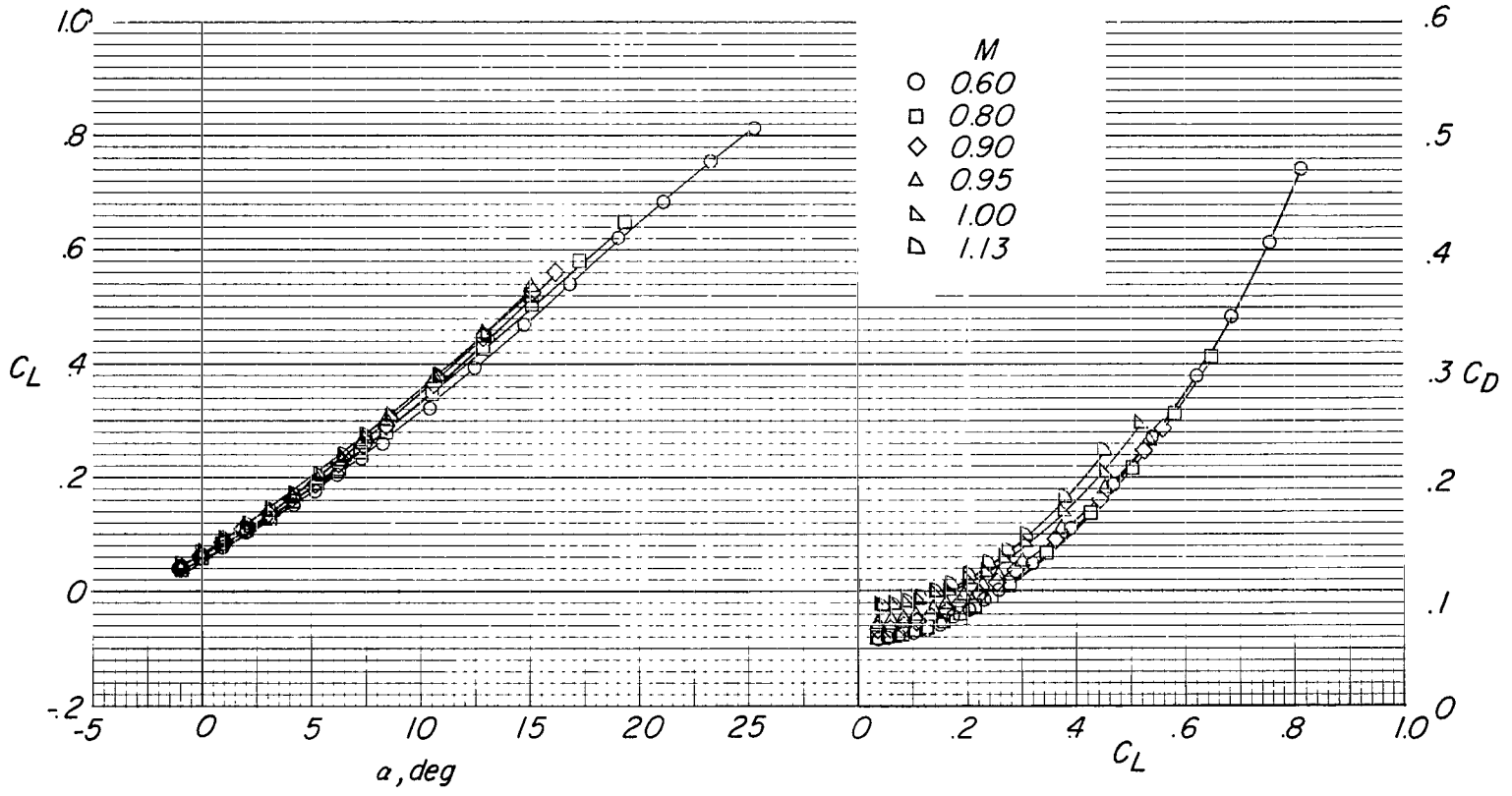

(a) Canard undeflected.

Figure 9.- Effects of increasing Mach number on longitudinal aerodynamic characteristics of configuration having wing panels swept back 80°, with canard and afterbody flaps on. Trailing-edge flaps off; $\delta_A = 100°$.

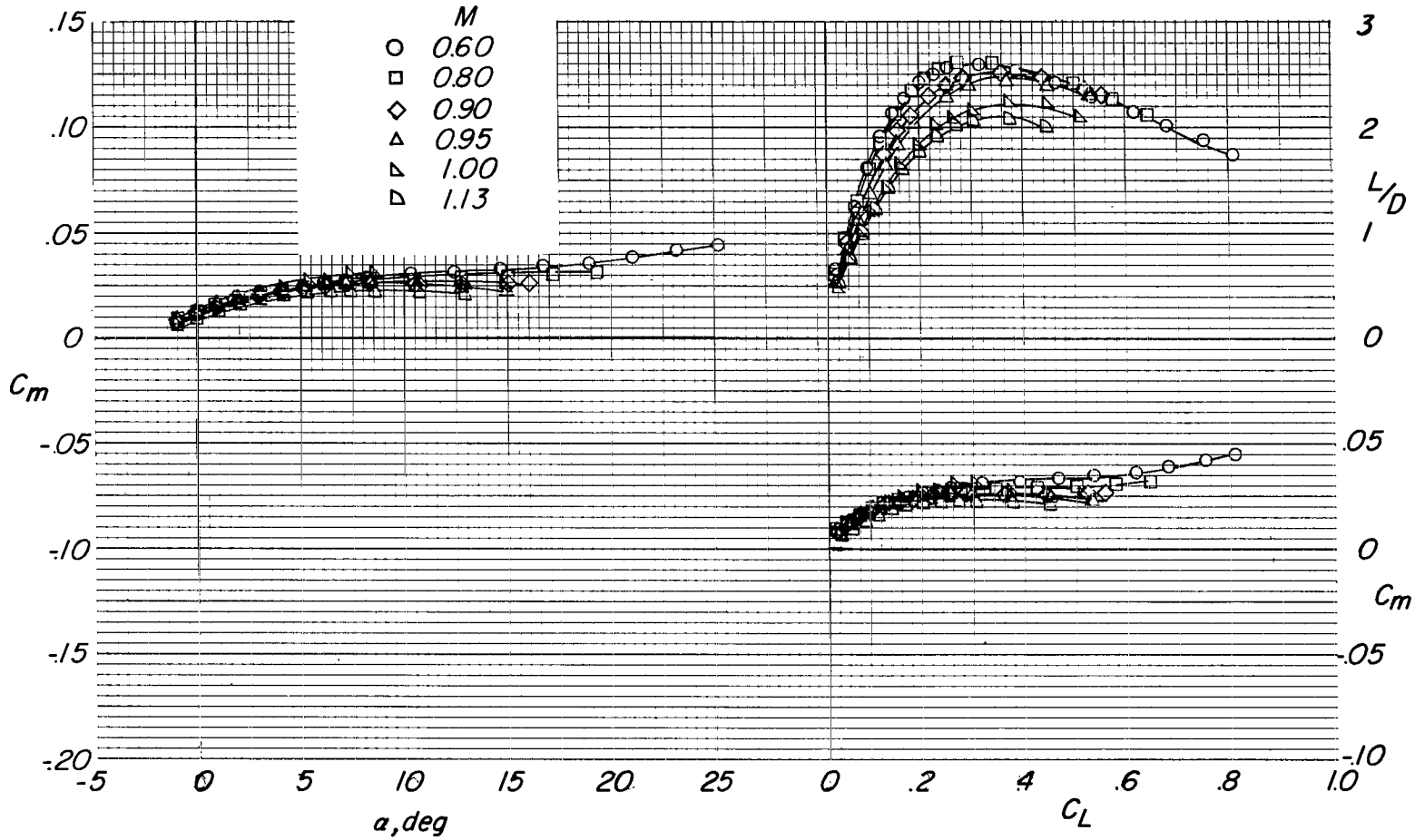

(a) Canard undeflected. Concluded.

Figure 9.- Continued.

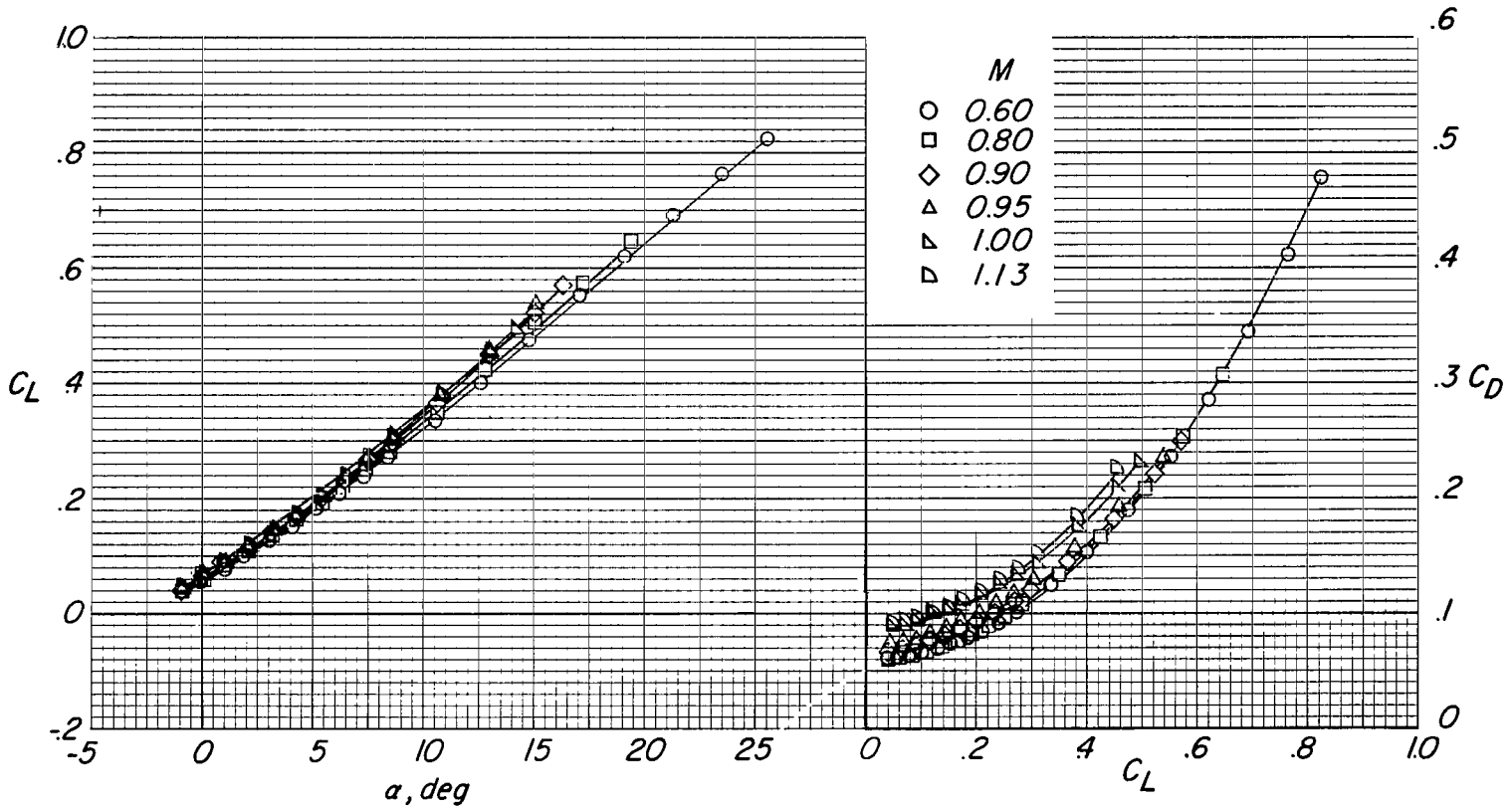

(b) Canard flaps deflected: $\delta_{f,c} = 30^\circ$, $\delta_{n,c} = -20^\circ$.

Figure 9.- Continued.

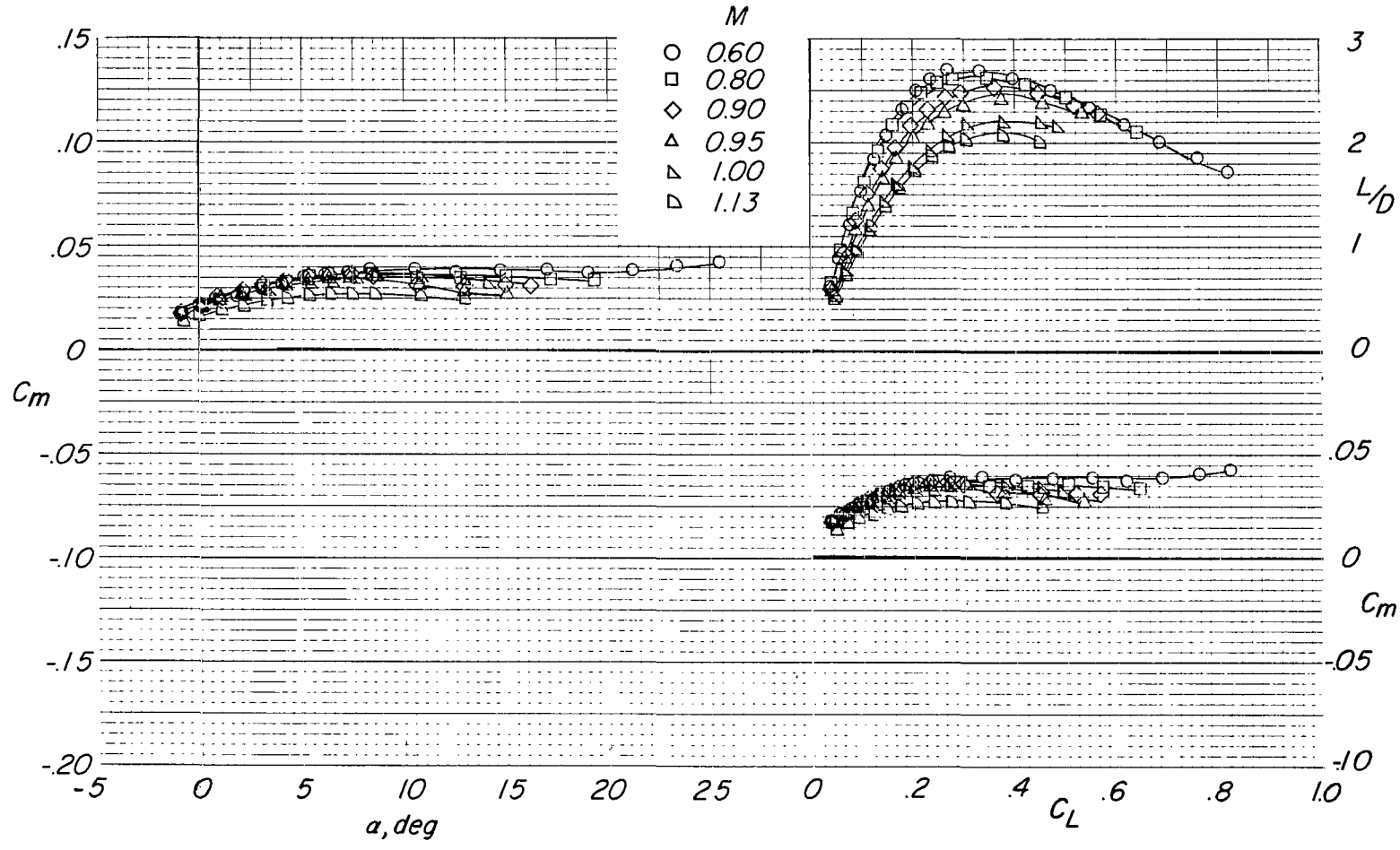

(b) Canard flaps deflected: $\delta_{f,c} = 30^{o}$, $\delta_{n,c} = -20^{o}$. Concluded.

Figure 9.- Concluded.

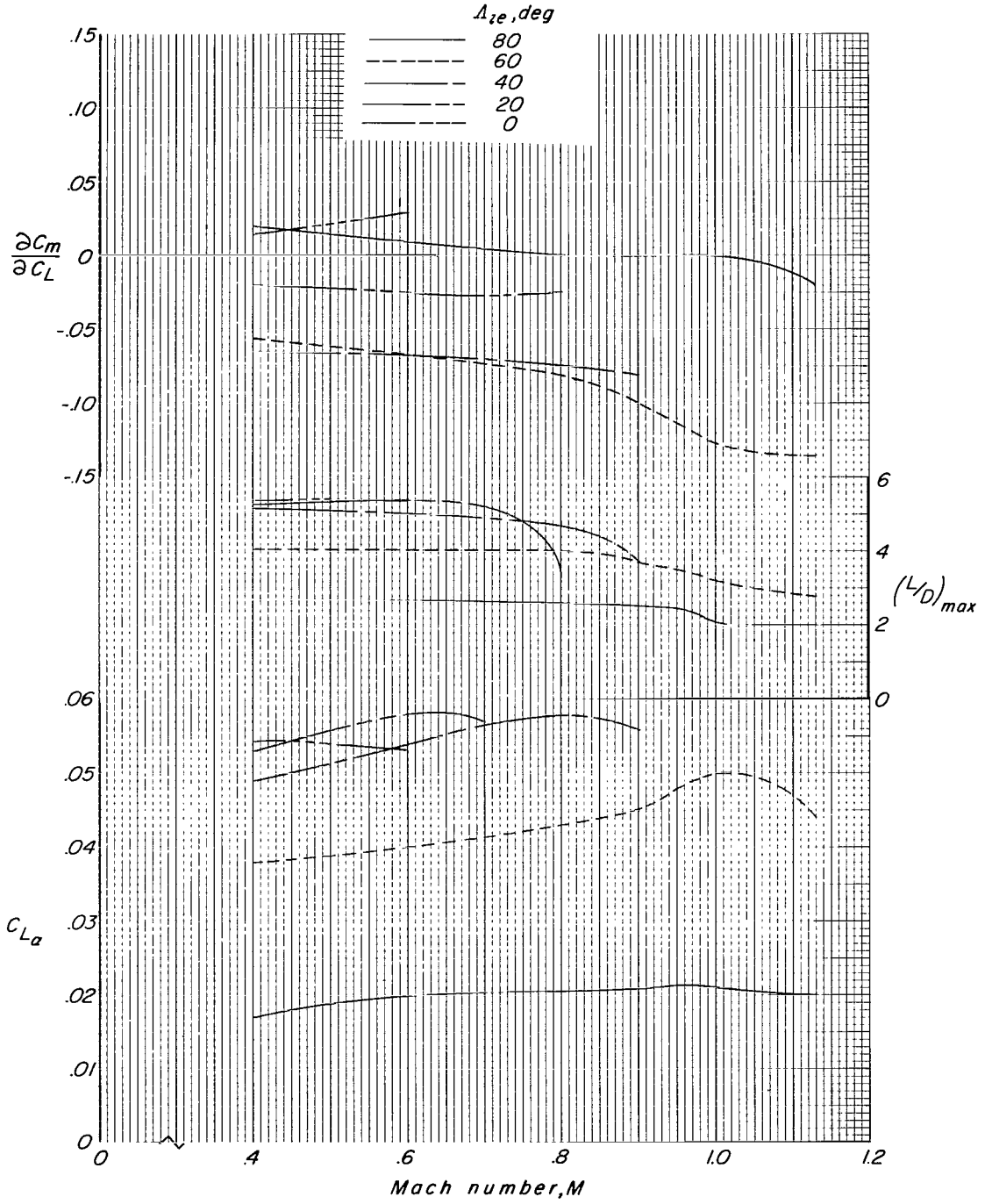

Figure 10.- Summary of effect of increasing Mach number on longitudinal aerodynamic parameters C_{L_α}, $(L/D)_{max}$, and $\partial C_m/\partial C_L$ for range of wing-panel sweeps. All controls off.

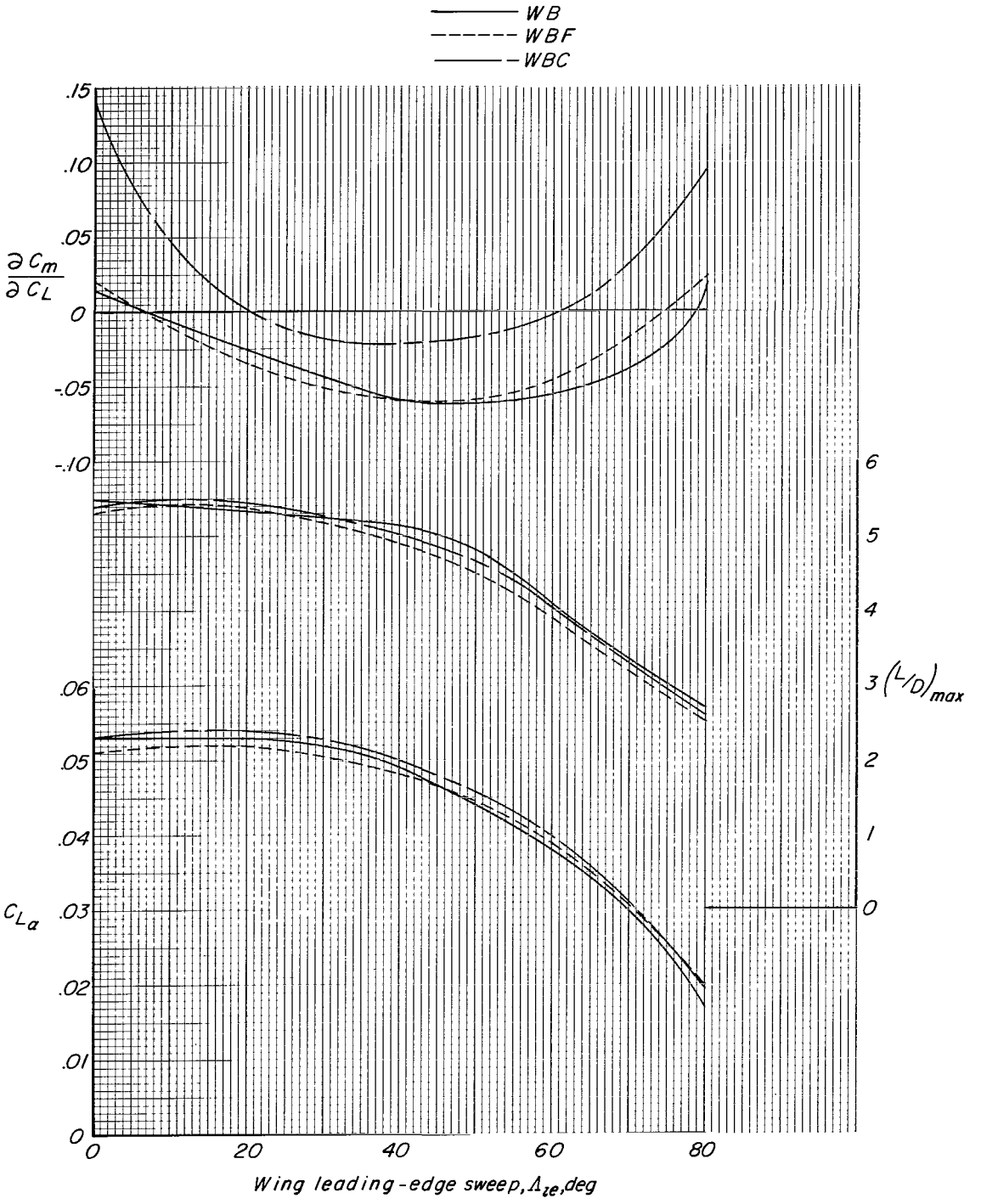

Figure 11.- Summary of longitudinal aerodynamic parameters C_{L_α}, $(L/D)_{max}$, and $\partial C_m/\partial C_L$ for each wing-panel sweep and for various longitudinal controls on basic configuration. M = 0.40; all controls at zero deflection.

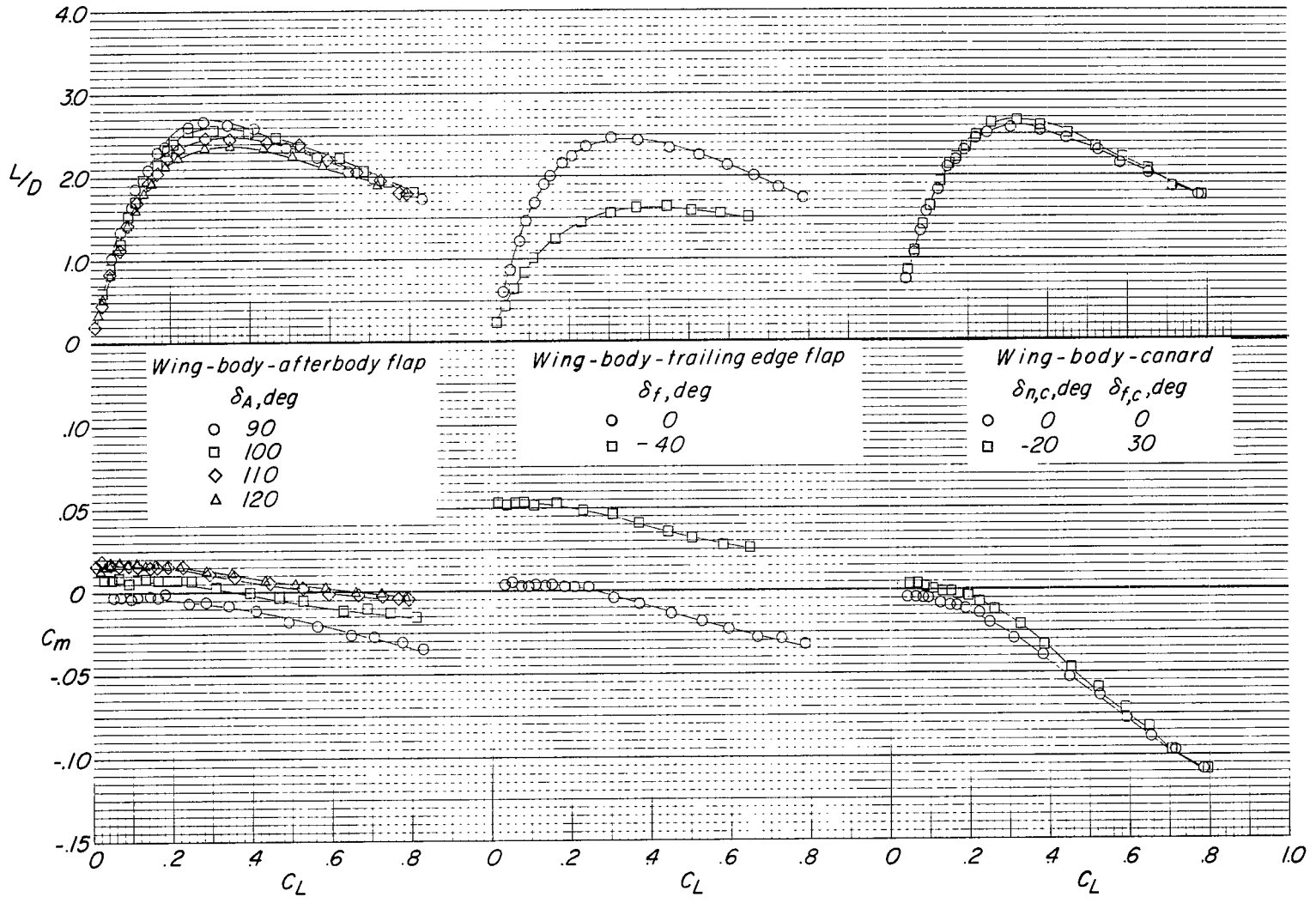

Figure 12.- Comparison of longitudinal trimmed lift and lift-drag ratio characteristics noted for canard, afterbody flap, and body trailing-edge flap configurations. M = 0.40; $\Lambda_{le} = 80^{\circ}$. (Moment reference point has been adjusted to render approximately -0.03c static margin at low lift for each configuration for comparison purposes.)

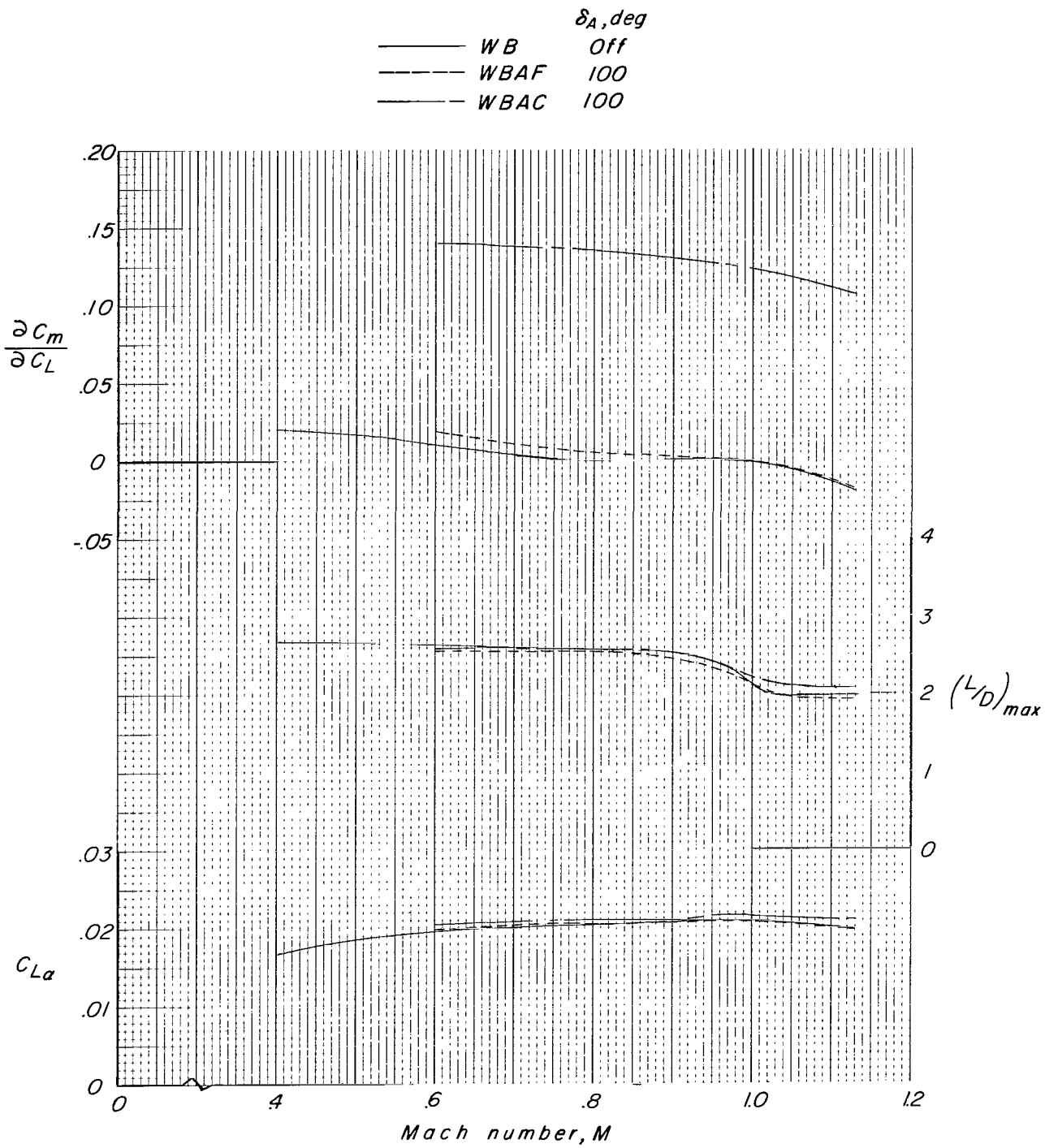

Figure 13.- Effects of Mach number on various longitudinal aerodynamic parameters for some of the configurations tested. $\Lambda_{le} = 80^\circ$. (Original moment reference.)

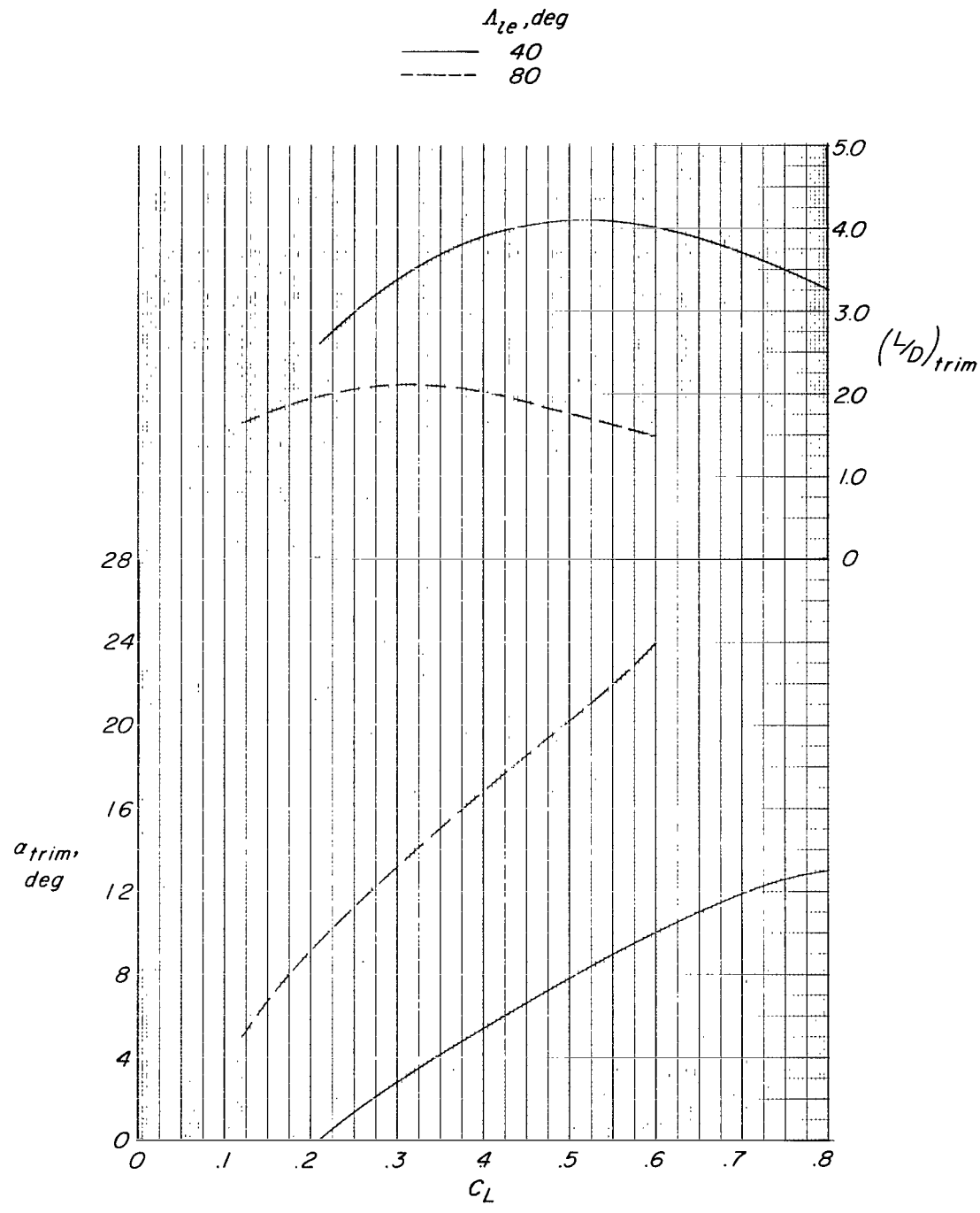

Figure 14.- Variation of trimmed L/D and α with increasing lift coefficient for configuration having afterbody flaps on, $\delta_A = 120^\circ$, and trailing-edge flaps deflected for control. M = 0.40. (Static margin adjusted to approximately -0.12c for each configuration.)